**Title**
New Transcriptional Regulators of Non-shivering Thermogenesis



**Author**
Dempersmier, Jon Michael

**Publication Date**
2015

Peer reviewed|Thesis/dissertation

# New Transcriptional Regulators of Non-shivering Thermogenesis

By

**Jon Michael Dempersmier Jr.**

A dissertation submitted in partial satisfaction of the

requirements for the degree of

**Doctor of Philosophy**

in

**Comparative Biochemistry**

in the

Graduate Division

of the

University of California, Berkeley

Committee in charge:

Professor Hei S. Sul, Chair
Professor Fenyong Liu
Professor James Olzmann
Professor Daniel K. Nomura

## ABSTRACT

**New Transcriptional Regulators of Non-shivering Thermogenesis**

by

**Jon Michael Dempersmier Jr.**

**Doctor of Philosophy in Comparative Biochemistry**

**University of California, Berkeley**

**Professor Hei S. Sul, Chair**

Unlike white adipose tissue (WAT), which stores excess energy as triglycerides, brown adipose tissue (BAT) burns fatty acids and glucose to produce heat. The thermogenic ability of BAT is due to the specialized inner mitochondrial proton transporter named uncoupling protein 1 (UCP1), which dissipates the proton motive force generated by the electron transport chain to create heat instead of ATP. Despite data suggesting that increasing BAT activity may be a promising antiobesity therapy, an inclusive model of the transcriptional regulation of thermogenic genes remain unclear. The aim of this dissertation work was to identify and characterize novel regulators of the UCP1 promoter and nonshivering thermogenesis.

Chapter 1 reviews BAT in both mice and human, profiling the basic mechanism of uncoupled respiration and cold-induced nonshivering thermogenesis. Unlike classical BAT, which has constitutive UCP1 expression, brown adipocyte-like cells arise in WAT depots following prolonged cold exposure and contribute to whole body thermogenic capacity. While having similar functions, these cells arise from different precursor populations, having unique gene signatures and potentially depot specific regulation. Human BAT resembles either classical BAT or brown adipocyte-like cells in a depot specific manner, with differing levels of basal UCP1 expression and expression profiles. Finally, known transcriptional and hormonal regulators of BAT are discussed.

Chapter 2 profiles my screening efforts to identify novel transcriptional regulators of the UCP1. Briefly, a library of over 1100 transcription factors was screened for activation of the UCP1 promoter. Expression profiling of the positive factors identified 6 novel, brown fat enriched transcriptional activators of UCP1. The first such transcription factor identified was the previously uncharacterized C2H2 type zinc-finger protein, Zfp516. Zfp516 is induced by cold where it binds and activates a brown fat gene program. Zfp516 ablation is embryonic lethal, but Zfp516 knockout embryos have little to no UCP1 expression and aberrant morphology. On the other hand, adipose specific transgenic overexpression in aP2-Zfp516 resulted in marked browning of inguinal WAT,

increased body temperature and whole body energy expenditure, and prevention of diet-induced obesity.

Chapter 3 profiles a second transcription factor identified in my screening efforts, the CCCH-type zinc finger protein, Zc3h10. Zc3h10, together with multiple cofactors, binds and activates the distal UCP1 promoter. Ablation of Zc3h10 results in defective BAT differentiation in cells, while adipose specific transgenic overexpression in aP2-Zc3h10 mice results in a lean phenotype.

Finally, chapter 4 concludes this work, discussing my findings in the context of the field of brown adipocyte biology and presents future directions and remaining questions.

This study has identified novel transcriptional regulators of UCP1, contributing significantly to the understanding of brown adipocyte biology and nonshivering thermogenesis, and providing new targets for future antiobesity therapeutics.

*To my grandparents, whose support, encouragement, and example have made me into the person I am today. And to my mom, my biggest cheerleader and number one supporter.*

**Table of Contents**

## List of Figures

## List of Tables

**Acknowledgements**

Graduate school truly has been the single hardest undertaking of my life, resulting in highs and lows, gray hairs, and tumultuous changes to myself, my family, and my life. It's been an incredible journey, made worthwhile by my co-commiserators, co-conspirators, and collaborators, all of whom I humbly thank for their role in this journey.

I would be remiss to not begin my acknowledgements by thanking my boss, mentor, and advisor, Hei Sook Sul, for her tireless effort, support, persistence with me and my project throughout my graduate career. I would also like to thank the members of my dissertation committee, Fengyong Lui, James Olzmann, and Daniel Nomura, for lending me their guidance and insight, both indirectly and directly, over the years.

I would not have been able to accomplish nearly as much as I have without the help and friendship of my amazing labmates, Carolyn Hudak and Olga Gulyaeva. Also, a special thanks to Yuhui Wang, whose years of molecular biology wisdom have assisted immeasurably in advancing my research.

To my friends, Cody Wilson, Mike Campbell, Travis Fahey, and Vanessa de la Rosa, thank you for your willingness to grab a beer with me and help me forget my troubles. And to Allison McQueen…you know what you did.

And finally, special thanks to my family, for understanding both when I do call and I don't call and believing in me every step of the way.

Chapter 1:

# Shades of Brown:

## A Model of Thermogenic Fat

**Shades of Brown: A Model of Thermogenic Fat**

**Abstract**

**Brown adipose tissue (BAT) is specialized to burn fuels to perform thermogenesis in defense of body temperature against cold. Recent discovery of metabolically active and relevant amounts of BAT in adult humans have made it a potentially attractive target for development of anti-obesity therapeutics. There are two types of brown adipocytes: classical brown adipocytes as well as brown adipocyte-like cells, so called beige/brite cells, that arise in white adipose tissue in response to cold and hormonal stimuli. These cells may derive from distinct origins, and while functionally similar, have different gene signatures. Here, we highlight recent advances in the understanding of brown and beige/brite adipocytes as well as transcriptional regulation for development and function of murine brown and beige/brite adipocytes focusing on EBF2, IRF4 and ZFP516, in addition to PRDM16 as a coregulator. We also discuss hormonal regulation of brown and beige/brite adipocytes including several factors secreted from various tissues, including BMP7, FGF21 and irisin, as well as those from BAT itself, such as Nrg4 and adenosine.**

**Introduction**

The pandemic rise in the prevalence of obesity, as well as its comorbidities, such as type 2 diabetes and cardiovascular diseases, has made it imperative to develop novel anti-obesity therapeutics. Obesity results from chronic excess of energy consumed through the diet versus energy expenditure through basal metabolism, physical exertion, and adaptive thermogenesis. Thus, successful therapies must involve either increasing energy expenditure or preventing absorption of calories from the diet, both of which have been used to limited success. One area of relative promise centers on targeting brown adipose tissue (BAT) to increase energy expenditure. Differing from white adipose tissue (WAT), which stores excess energy from the diet as triglycerides, BAT is a thermogenic organ, metabolizing both fatty acids and glucose to produce heat to maintain homoeothermy. The thermogenic activity of BAT is possible due to the presence of a BAT-specific mitochondrial proton transport protein, uncoupling protein 1 (UCP1), which uncouples the mitochondrial proton gradient from ATP synthesis and generates heat. While existence of BAT in infants as well as discrete populations of adult humans had been shown many years ago [1], recent findings using $^{18}$fluoro 2-deoxyglucose positron emission tomography (FDG-PET) verified the presence of metabolically active BAT in human adults [2,3]. Thus, developing BAT may provide an attractive new target for prevention/treatment of obesity. A better understanding of BAT development and function has the potential to improve the health of millions of Americans and others affected by obesity and its associated disorders.

**Thermogenesis: A Sum of all BATs**

Earliest work on BAT centered on its function in thermogenesis, identifying the basic tenets of BAT activation in response to cold. Upon cold-exposure, sympathetic nervous system (SNS) innervating BAT releases norepinephrine, which, via $\beta_3$-adrenergic receptor (AR)-cAMP-PKA pathway, stimulates lipolysis to produce fatty acids for oxidation. These fatty acids can also allosterically activate UCP1-mediated uncoupling, as UCP1 functions as a $H^+$/ fatty acid symporter [4,5]. Furthermore, via CREB/ATF2, stimulation of $\beta_3$-AR induces BAT-enriched genes, including UCP1 [6]. $\beta_3$-AR stimulation also increases expression of PGC1α, which is critical for mitochondrial biogenesis to support BAT thermogenesis.

Classical brown adipocytes come from a developmental lineage distinct from WAT, arising from $Myf5^+$/$Sca\text{-}1^+$/$Pax7^+$ cells of the dermomyotome, a common progenitor of skeletal muscle and dermis [7–9]. Following treatment with bone morphogenic protein-7 (BMP7), these precursor cells can be induced to differentiate into brown adipocytes [10]. While many transcriptional and hormonal regulators of brown adipocyte differentiation and thermogenesis have been identified as discussed below, commitment to brown preadipocytes from multipotent precursors is yet to be clearly defined.

As our understanding of BAT development and function has progressed, it became apparent that non-shivering thermogenesis of BAT is only half of the coin. The earliest reports of the presence of brown adipocyte-like cells in WAT depots in mice following cold acclimation stretch back over 30 years [11]. Indeed, various treatments have been shown to result in the rise of $UCP1^+$ cells in WAT, but the physiological relevance of these cells has been poorly understood. However, seminal work by Schultz et al. showed that severing sympathetic neurons to brown fat or blocking BAT development both lead to compensatory rise in brown-like adipocytes in WAT [12]. Thus, WAT depots can act as reserve thermogenic pool of cells for cold adaptation, although the overall contribution to whole body thermogenesis is not known. The ability for cells within a WAT depot to give rise to $UCP1^+$ cells varies depot by depot, as well as with different strains of mice. With chronic cold exposure, all depots are capable of undergoing some degree of browning [13]. Thus, total thermogenic capacity for mice might be dependent on the contribution of all $UCP1^+$ cells in all adipose organs rather than BAT alone.

Recent characterization of the brown adipocyte-like cells in WAT depots has revealed them to be distinct from classic brown adipocytes. These so called beige or brite cells (brown-in-white) have low expression levels of UCP1 at ambient temperature, but are greatly induced upon cold exposure. The process of "browning" or recruitment is primarily under sympathetic control and ablation of β3-adrenergic receptor has been reported to severely block formation of beige/brite adipocytes in WAT depots. The browning process, however, is one of much debate as to whether cold challenge leads to recruitment of preadipocytes that are distinct from white precursors to differentiate into

UCP1$^+$ adipocytes, or whether white adipocytes present in the tissue are interconverted to become UCP1$^+$ cells. Indeed, early work by Himms-Hagen et al. showed that following 7 day-treatment of the β3 agonist, CL-316,243, the majority of multilocular cells, indicative of beige/brite adipocytes, were negative for BrdU staining, suggesting interconversion as the primary pathway for induction of UCP1$^+$ cells [14]. However, using pulse-chase experiments employing the adiponectin based AdipoChaser model, Wang et al. recently showed that adipocytes in subcutaneous or inguinal WAT (iWAT), that were indelibly labeled with LacZ prior to cold exposure, did not express UCP1 following 3 days of cold exposure. Thus, UCP1 expression was confined to LacZ$^-$ cells, suggesting *de novo* differentiation of distinct precursor cell populations [15]. Interestingly, this phenomenon was limited to iWAT. In epididymal WAT (eWAT), cold exposure led to *de novo* adipogenesis without UCP1 expression. This is contradictory to the observation that cold acclimation led to substantial browning of almost all WAT depots [13,16]. On the other hand, Lee et al. reported that, while the majority of browning of iWAT resulted from recruitment of preadipocytes to become UCP1$^+$ adipocytes, thermogenic adipocytes in eWAT arose from interconversion from white adipocytes [17]. Could there be a depot specific mechanism for browning or is there a common intermediate for thermogenic cells? Perhaps, the differences in adrenergic innervation of the two depots may lead to a requirement for noradrenergic fiber branching prior to recruitment of beige/brite adipocytes in eWAT [18]. Interestingly, Rosenwald et al. showed that recruited beige/brite adipocytes were able to revert back to white adipocytes once the stimulus was removed. When restimulated, these same cells were converted back again to thermogenic beige/brite adipocytes [19]. The authors also showed that upon restimulation, a percentage of the cells positive for UCP1 were not labeled upon the original cold stimulation, potentially signifying the recruitment of new beige/brite adipocytes. Whether these adipocytes are recruited from progenitor populations signifying *de novo* recruitment or indicative of a limitation of the system is unclear. Regardless, the ability for beige/brite cells to interconvert to white adipocytes makes discerning the mechanism for browning difficult.

In an attempt to identify precursors of the brown-like cells in WAT, Wu et al. performed clonal expansion of preadipocytes of iWAT and identified non-thermogenic and thermogenic precursor populations each with unique gene expression signatures. The thermogenic lines expressed many common genes with those of BAT (UCP1, PGC1α) as well as beige specific genes such as Tmem26, Tbx1, CD137, and CD40 [20]. Interestingly, CD40 ligand (CD40L) in humans has been correlated with obesity [21]. Disruption of CD40 signaling in mice has been reported to increase UCP1 expression in BAT and to protect against diet induced obesity [22]. With this contradictory observation, the beige markers so far identified need to be further characterized and verified. Further complicating the matter, Lee et al. isolated PDGFRα$^+$ cells from eWAT and found them to be bipotent precursors that could differentiate into either brown or white adipocytes *in vitro*.

However, transplants of these cells into mice resulted in only UCP1$^-$ white adipocytes, even after CL-316,243 treatment [17].

While a small subset of cells in WAT depots have been reported to be Myf5$^+$, recent studies have shown that these cells had a reduced capacity to become brown-like adipocytes [23,24]. On the other hand, using a UCP1-promoter reporter system, Long et al. identified a population of beige/brite adipocytes that arose from cells that are positive for Myh11, a smooth muscle-like marker. However, within the iWAT depot, not all of the UCP1$^+$ cells were Myh11$^+$, suggesting that, even within a single depot, heterogeneity of beige cells may exist. Further studies are necessary to define whether beige adipocytes are a distinct population of cells within WAT depots and whether these cells arise from distinct precursors, and if they do, to define the lineage of these cells (Figure 1).

**Human BAT: Brown, Beige, or Shades of Brown**

As mentioned above, the classic dogma in human BAT centers around the previously accepted fact that interscapular BAT, anatomically similar to that in rodents, is abundant in infants but decreases with age [25]. However, reports of detectable amounts in young, lean adults following cold stimulation do exist [26]. Recently, prospective studies using FDG-PET scanning identified UCP1$^+$ BAT in a majority of adults in the cervical, supraclavicular, and paravertebral areas, which was responsive to cold and negatively regulated by warm environment, sympathetic blockade, or dietary intervention [2,27,28]. These findings showed a great therapeutic potential, as many groups have shown that increased BAT activity and function was protective against diet-induced obesity and insulin resistance in mice. Moreover, recent human studies showed similar observations. Cold exposure in humans led up to a 12-fold increase in glucose uptake, an increase in energy expenditure, and improved insulin sensitivity [29,30]. The caveat to these studies is that the beneficial effects of cold exposure were based on having measureable amounts of human BAT. Yoneshiro et al. reported that spending 2 hours per day at 17°C for 6 weeks resulted in significant recruitment of BAT in the majority of subjects, leading to an increase in cold induced thermogenesis and a decrease in body fat mass, which was proportional to BAT activity [31]. Cooling subjects for extended periods of time below thermoneutrality, but not to the point of shivering, showed the prevalence of BAT to be close to 100% and thus individualized cold training could be a viable anti-obesity therapeutic [32]. However, therapeutic use of b-agonists or other sympathomimetics could not be used due to either inefficacy or cardiovascular side effects, including increased risk of cardiac events [33–35]. More research is needed to identify new therapeutics for increasing BAT recruitment and activity.

Understanding the nature of human BAT and whether it resembles classic murine brown or beige/brite cells is critical for therapeutics development, and is the subject of debate [36]. Early work on this issue using BAT depots identified by FGD-PET [20,37], showed similar results that human BAT expresses both TMEM26 and CD137, murine

beige/brite markers, but not LHX8 or ZIC1, iBAT selective markers. Interestingly, later work by Jespersen et al. on supraclavicular biopsies found elevated expression of LHX8 and ZIC1, as well as TMEM26 and CD137, suggesting that both beige/brite and brown adipocytes may be present. Cypess et al. profiled adipose tissue from 5 different sites in patients found that deep neck fat expressed high levels of iBAT markers, ZIC1and LHX8, as well as UCP1, while superficial fat depots expressed WAT selective HOXC9 and leptin. Interestingly, all depots, including iBAT, were found to express the beige markers, TMEM26 and CD137 [3,25]. These data suggest that TMEM26 and CD137 may be better described as pan-thermogenic adipocyte markers in humans, rather than beige/brite markers. Regardless, the presence of $ZIC1^{+}/LHX8^{+}$ depots suggests that adult humans have both beige/brite and brown adipocytes and thus both tissues may have therapeutic importance. However, the role of ZIC1 and LHX8 in thermogenesis is largely unexplored and thus, expression of these genes may not constitute a functional difference between beige and brown adipocytes.

**Transcriptional Regulation of Brown Adipogenesis**

Numerous transcription factors, metabolites, and signaling molecules have been implicated in activating brown adipocytes and/or brown fat differentiation [38,39]. Here, we highlight several recently identified key players in BAT gene expression and development, and regulation of non-shivering thermogenesis.

Earliest work on identifying critical transcriptional regulators of thermogenesis centered on the regulation of the UCP1 promoter. Sympathetic regulation of UCP1 in response to cold has been defined to be mediated by βAR-cAMP-PKA through CREB/ATF2 via p38 [40,41]. Both CREB and ATF2 could bind to the cAMP response element (CRE) at the proximal UCP1 promoter as well as at the conserved DNase I hypersensitive enhancer region at -2.5 kb upstream of the transcription start site [42,43]. This enhancer region also contains common response elements, including thyroid hormone response element (TRE), peroxisome proliferator-activated receptor response element (PPRE), as well as retinoic acid response element (RARE). However, all of the factors that can bind to these elements are somewhat ubiquitous and thus do not easily explain BAT-specific and sympathetically regulated expression of UCP1.

One of the first to be reported as a BAT-enriched regulator of thermogenesis is PR-domain containing protein 16 (PRDM16). PRDM16 has been shown to function as a coactivator of brown adipogenesis through interaction with several transcription factors, including C/EBPβ, CtBPs, PGC1α, and PPARγ, as well as the H3K9 histone methyltransferase, EHMT1, to drive brown fat/ muscle precursors toward a brown fat lineage [44–46]. Indeed, in fibroblasts and C2C12 myoblasts, ectopic expression of PRDM16 and C/EBPβ was sufficient to drive a brown fat transcription program leading to functional brown adipocytes [47]. However, conditional deletion of PRDM16 in two different mouse models using adiponectin-Cre or Myf5-Cre found PRDM16 to be

dispensable for BAT development. However, these mice showed defects in BAT maintenance during aging. In addition, ablation of PRDM16 by adiponectin-Cre in WAT blocked recruitment of beige adipocytes demonstrating a role of PRDM16 in browning of WAT [48,49]. More work is needed to better understand the role of PRDM16 in BAT development and browning of WAT.

In an attempt to identify brown fat specific PPARγ binding sites, Rajakumari et al. performed ChIP-seq on PPARγ and found that PPARγ sites in BAT coincided with early B-cell factor (EBF) binding sites, particularly within the UCP1 and PRDM16 promoters. They further showed that loss of EBF2 of the EBF family of transcription factors, resulted in a complete loss of BAT characteristics, with little to no expression of UCP1, PRDM16, or CideA, while general adipogenic markers, such as PPARγ, were unaffected [50]. Cell sorting for $GFP^+$ cells in EBF2/GFP mice showed that EBF2 reliably marked preadipocytes of brown adipogenic potential present in both BAT and iWAT [51]. Given the heterogeneity of beige cells within tissues, it would interesting to see if all $UCP1^+$ cells in various WAT depots are derived from $EBF2^+$ cells.

Cold inducible regulation of UCP1 was thought to be, along with CREB/ATF2, through the participation of PGC1α, a coactivator central to mitochondrial biogenesis [52,53]. While original reports of PGC1α null mice showed reduced thermogenic capacity, recent adipocyte-specific ablation of PGC1α resulted in only mild cold intolerance and insulin resistance [54,55]. On the other hand, ablation of a PGC1α interacting partner, IRF4, led to a more severe defect in thermogenesis and energy expenditure [56]. The role IRF4 plays in BAT development is currently unclear, since IRF4 has also been shown to repress adipogenesis as well as expression of general adipocyte markers including PPARγ and FABP4 [57].

Recently, by high throughput screening using the proximal -5.5kb of the UCP1 promoter, Dempersmier et al. identified the previously uncharacterized transcription factor, Zfp516, as a BAT-enriched, cold-inducible regulator critical for expression of BAT genes and BAT development, as well as browning of iWAT. Ablation of Zfp516 led to impaired BAT development with no detectable UCP1 expression. Conversely, overexpression of Zfp516 in aP2-Zfp516 transgenic mice showed a drastic browning of iWAT with an over 80% increase in tissue oxygen consumption rate. Moreover, overexpression of Zfp516 also resulted in prevention of diet-induced obesity and improved glucose tolerance and insulin sensitivity. Furthermore, ectopic expression of Zfp516 was sufficient to drive C2C12 myoblasts to becoming brown adipocytes [58]. As a BAT-enriched, sympathetically regulated transcription factor, Zfp516 may prove to be a central regulator of BAT development and browning of iWAT and thus for non-shivering thermogenesis (Figure 2).

**Signaling in BAT: A convergence of signals and outputs**

As an energetically expensive process, thermogenesis in brown and beige adipocytes is under tight hormonal and environmental control. Outside of sympathetic regulation of BAT and browning of iWAT, early work by Tseng et al. identified BMP7 as a critical regulator of BAT development. Ablation of either BMP7 or its receptor led to severely blunted BAT development and impaired thermogenesis [12,59]. While the source of BMP7 driving BAT development is unclear, many tissues, including heart (natriuretic peptides), muscle (Irisin), liver (FGF21), hypothalamus (Bmp8b), thyroid (T4), blood vessels (VEGF), and alternatively activated macrophages (norepinephrine), have been found to signal BAT and WAT to promote thermogenesis and browning [34,60,61]. Recent work has also highlighted that signaling from brown adipocytes itself can play a role in thermogenesis. Gnad et al. reported that adenosine, released from sympathetic nerves as well as from BAT following the release of norepinephrine, to increase the response to norepinephrine through the $G_s$- coupled $A_{2A}$ receptor in BAT. Thus, adenosine was shown to act as a feed forward loop, increasing cAMP levels to further activate thermogenic genes [62]. Ablation of $A_{2A}$ receptor resulted in an attenuated sympathetic signaling and oxygen consumption in response to cold or β-agonist treatment. However, it has not been shown whether adenosine signaling is required for browning in mice. Regardless, relevant for potential therapeutics, adenosine has already been shown to increase lipolysis and UCP1 expression in human BAT.

BAT-released signaling molecules can also play a role in other tissues. Wang et al. identified Nrg4 as a BAT enriched secreted protein. Nrg4 was reported to primarily signal through the liver, where it down regulated a panel of genes involved in *de novo* lipogenesis, including *Srebp1c*, *Acc1*, *Scd1*, and *Fasn*. While not affecting thermogenesis, Nrg4 was shown to decrease insulin resistance and hepatosteatosis via gain-of- and loss-of-function studies in mice [63]. However, the physiological importance and possible nutritional response of Nrg4 have not yet been assessed. Perhaps Nrg4 expression inhibits *de novo* lipogenesis to conserve fuels for BAT in times of cold challenge. In addition to Nrg4, other potential BAT-enriched secreted factors that may affect insulin resistance and metabolic homeostasis need to be identified and studied.

**Conclusions and Future Outlook**

The affirmation of the existence BAT in human adults has led to an explosion of new information, highlighting the therapeutic potential of BAT. Work on human cold training has shown strong evidence that BAT is prevalent, present in almost all humans to varying amounts, and may be potentially useful in treatment of obesity and type 2 diabetes. However, the inconvenience of cold training makes the “magic pill” to activating hBAT is still the Holy Grail in the field. Understanding the regulation of thermogenesis is, therefore, essential for development of novel therapeutics. Indeed,

further work on hormonal and transcriptional regulation of beige/brite and brown adipose development may lead to new insights and therapeutic targets in the future.

**Acknowledgements**

The work from the authors' laboratory was supported by DK095338 to H.S.S.

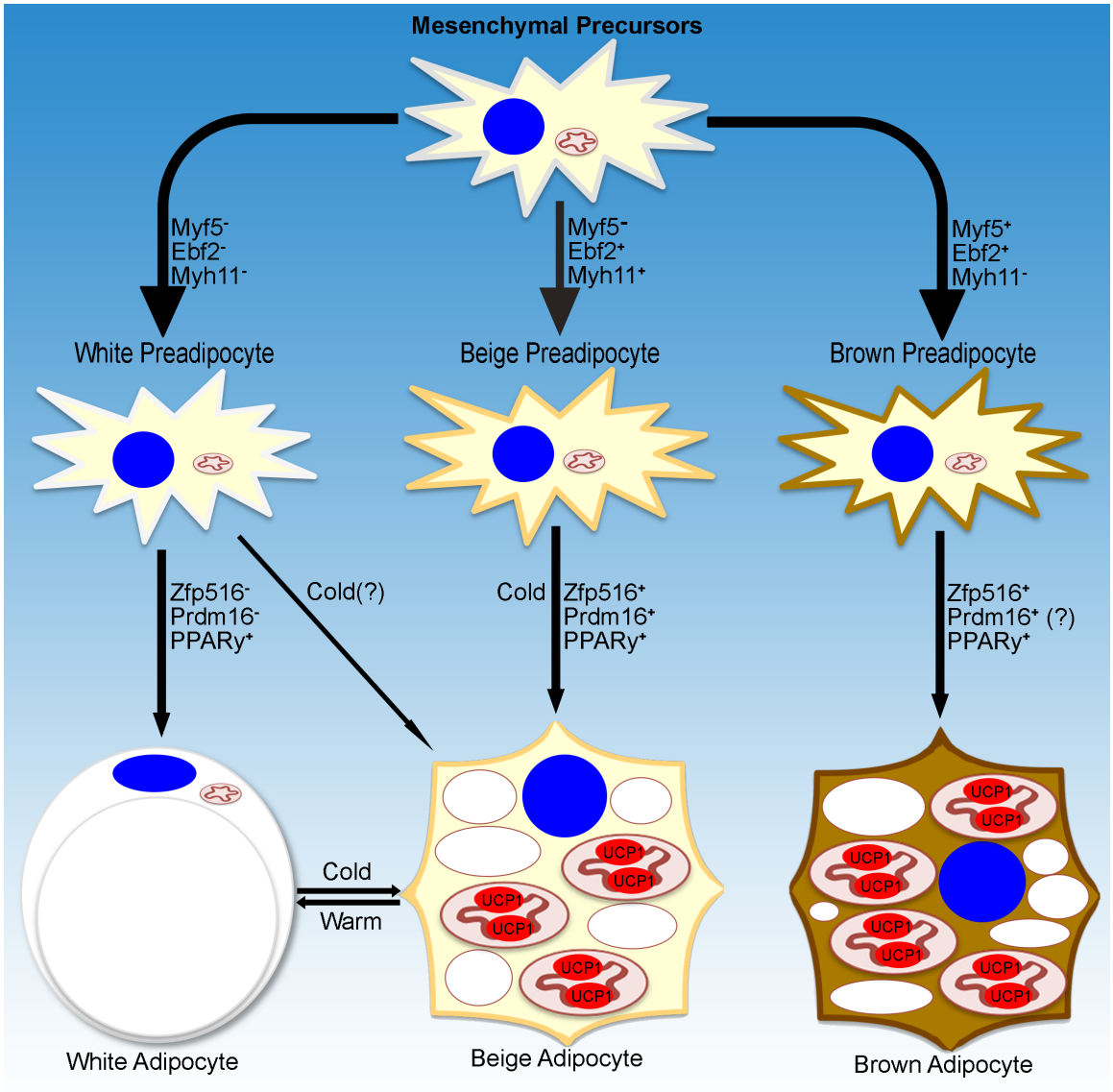


**Figure 1. Transcriptional Regulation of Adipocyte Development.** Schematic representation of markers denoting specific lineages of thermogenic adipocytes. Transcriptional regulators and environmental cues for adipocyte development discussed in the text are listed as well.

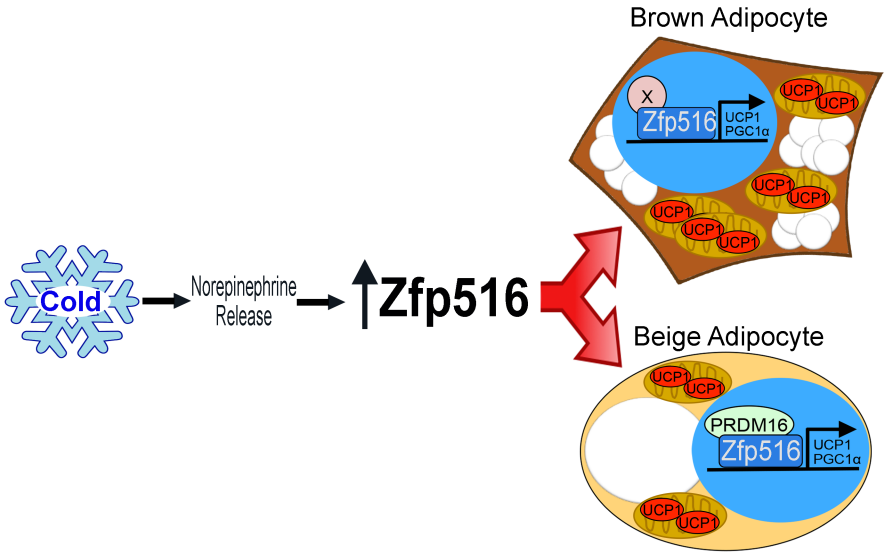


**Figure 2. Regulation of Thermogenic Adipocytes by Zfp516.** Cold exposure leads to increased Zfp516 levels resulting in induction of thermogenic genes in beige and brown adipocytes.

## References


1. Huttunen, P., Hirvonen, J. & Kinnula, V. The occurrence of brown adipose tissue in outdoor workers. *Eur. J. Appl. Physiol.* **46,** 339–345 (1981).

2. Cypess, A. M. *et al.* Identification and importance of brown adipose tissue in adult humans. *N. Engl. J. Med.* **360,** 1509–1517 (2009).

3. Cypess, A. M. *et al.* Anatomical localization, gene expression profiling and functional characterization of adult human neck brown fat. *Nat. Med.* **19,** 635–639 (2013).

4. Fedorenko, A., Lishko, P. V. & Kirichok, Y. Mechanism of fatty-acid-dependent UCP1 uncoupling in brown fat mitochondria. *Cell* **151,** 400–413 (2012).
5. Silva, J. E. Thermogenic mechanisms and their hormonal regulation. *Physiol. Rev.* **86,** 435–464 (2006).

6. Collins, S., Yehuda-Shnaidman, E. & Wang, H. Positive and negative control of Ucp1 gene transcription and the role of β-adrenergic signaling networks. *Int. J. Obes. 2005* **34 Suppl 1,** S28–33 (2010).

7. Gensch, N., Borchardt, T., Schneider, A., Riethmacher, D. & Braun, T. Different autonomous myogenic cell populations revealed by ablation of Myf5-expressing cells during mouse embryogenesis. *Dev. Camb. Engl.* **135,** 1597–1604 (2008).

8. Lepper, C. & Fan, C.-M. Inducible lineage tracing of Pax7-descendant cells reveals embryonic origin of adult satellite cells. *Genes. N. Y. N 2000* **48,** 424–436 (2010).

9. Seale, P. *et al.* PRDM16 controls a brown fat/skeletal muscle switch. *Nature* **454,** 961–967 (2008).

10. Schulz, T. J. *et al.* Identification of inducible brown adipocyte progenitors residing in skeletal muscle and white fat. *Proc. Natl. Acad. Sci. U. S. A.* **108,** 143–148 (2011).

11. Young, P., Arch, J. R. S. & Ashwell, M. Brown adipose tissue in the parametrial fat pad of the mouse. *FEBS Lett.* **167,** 10–14 (1984).

12. Schulz, T. J. *et al.* Brown-fat paucity due to impaired BMP signalling induces compensatory browning of white fat. *Nature* **495,** 379–383 (2013).

13. Cinti, S. The adipose organ: morphological perspectives of adipose tissues. *Proc. Nutr. Soc.* **60,** 319–328 (2001).

14. Himms-Hagen, J. *et al.* Multilocular fat cells in WAT of CL-316243-treated rats derive directly from white adipocytes. *Am. J. Physiol. - Cell Physiol.* **279,** C670–C681 (2000).

15. Wang, Q. A., Tao, C., Gupta, R. K. & Scherer, P. E. Tracking adipogenesis during white adipose tissue development, expansion and regeneration. *Nat. Med.* **19,** 1338–1344 (2013).

16. Vitali, A. *et al.* The adipose organ of obesity-prone C57BL/6J mice is composed of mixed white and brown adipocytes. *J. Lipid Res.* **53,** 619–629 (2012).

17. Lee, Y.-H., Petkova, A. P., Mottillo, E. P. & Granneman, J. G. In vivo identification of bipotential adipocyte progenitors recruited by β3-adrenoceptor activation and high-fat feeding. *Cell Metab.* **15,** 480–491 (2012).

18. Murano, I., Barbatelli, G., Giordano, A. & Cinti, S. Noradrenergic parenchymal nerve fiber branching after cold acclimatisation correlates with brown adipocyte density in mouse adipose organ. *J. Anat.* **214,** 171–178 (2009).

19. Rosenwald, M., Perdikari, A., Rülicke, T. & Wolfrum, C. Bi-directional interconversion of brite and white adipocytes. *Nat. Cell Biol.* (2013). doi:10.1038/ncb2740

20. Wu, J. *et al.* Beige adipocytes are a distinct type of thermogenic fat cell in mouse and human. *Cell* **150,** 366–376 (2012).

21. Poggi, M. *et al.* The inflammatory receptor CD40 is expressed on human adipocytes: contribution to crosstalk between lymphocytes and adipocytes. *Diabetologia* **52,** 1152–1163 (2009).

22. Chatzigeorgiou, A. *et al.* Blocking CD40-TRAF6 signaling is a therapeutic target in obesity-associated insulin resistance. *Proc. Natl. Acad. Sci.* **111,** 2686–2691 (2014).

23. Sanchez-Gurmaches, J. *et al.* PTEN loss in the Myf5 lineage redistributes body fat and reveals subsets of white adipocytes that arise from Myf5 precursors. *Cell Metab.* **16,** 348–362 (2012).

24. Shan, T. *et al.* Distinct populations of adipogenic and myogenic Myf5-lineage progenitors in white adipose tissues. *J. Lipid Res.* **54,** 2214–2224 (2013).

25. Lidell, M. E. *et al.* Evidence for two types of brown adipose tissue in humans. *Nat. Med.* **19,** 631–634 (2013).

26. Cypess, A. M., Haft, C. R., Laughlin, M. R. & Hu, H. H. Brown fat in humans: consensus points and experimental guidelines. *Cell Metab.* **20,** 408–415 (2014).

27. Van Marken Lichtenbelt, W. D. *et al.* Cold-activated brown adipose tissue in healthy men. *N. Engl. J. Med.* **360,** 1500–1508 (2009).

28. Virtanen, K. A. *et al.* Functional brown adipose tissue in healthy adults. *N. Engl. J. Med.* **360,** 1518–1525 (2009).

29. Chondronikola, M. *et al.* Brown Adipose Tissue Improves Whole-Body Glucose Homeostasis and Insulin Sensitivity in Humans. *Diabetes* **63,** 4089–4099 (2014).

30. Orava, J. *et al.* Different Metabolic Responses of Human Brown Adipose Tissue to Activation by Cold and Insulin. *Cell Metab.* **14,** 272–279 (2011).

31. Yoneshiro, T. *et al.* Recruited brown adipose tissue as an antiobesity agent in humans. *J. Clin. Invest.* **123,** 3404–3408 (2013).

32. Van der Lans, A. A. J. J. *et al.* Cold-activated brown adipose tissue in human adults: methodological issues. *Am. J. Physiol. Regul. Integr. Comp. Physiol.* **307,** R103–113 (2014).

33. Cypess, A. M. *et al.* Cold but not sympathomimetics activates human brown adipose tissue in vivo. *Proc. Natl. Acad. Sci. U. S. A.* **109,** 10001–10005 (2012).

34. Villarroya, F. & Vidal-Puig, A. Beyond the Sympathetic Tone: The New Brown Fat Activators. *Cell Metab.* **17,** 638–643 (2013).

35. Yen, M. & Ewald, M. B. Toxicity of weight loss agents. *J. Med. Toxicol. Off. J. Am. Coll. Med. Toxicol.* **8,** 145–152 (2012).

36. Scheele, C., Larsen, T. J. & Nielsen, S. Novel nuances of human brown fat. *Adipocyte* **3,** 54–57 (2014).

37. Sharp, L. Z. *et al.* Human BAT possesses molecular signatures that resemble beige/brite cells. *PloS One* **7,** e49452 (2012).

38. Nedergaard, J. & Cannon, B. The Browning of White Adipose Tissue: Some Burning Issues. *Cell Metab.* **20,** 396–407 (2014).

39. Wu, J., Cohen, P. & Spiegelman, B. M. Adaptive thermogenesis in adipocytes: is beige the new brown? *Genes Dev.* **27,** 234–250 (2013).

40. Cannon, B. & Nedergaard, J. Brown adipose tissue: function and physiological significance. *Physiol. Rev.* **84,** 277–359 (2004).

41. Cao, W., Medvedev, A. V., Daniel, K. W. & Collins, S. β-Adrenergic Activation of p38 MAP Kinase in Adipocytes cAMP induction of the uncoupling protein 1 (UCP1) gene requires p38 map kinase. *J. Biol. Chem.* **276,** 27077–27082 (2001).

42. Klingenspor, M. Cold-induced recruitment of brown adipose tissue thermogenesis. *Exp. Physiol.* **88,** 141–148 (2003).

43. Rim, J. S. & Kozak, L. P. Regulatory motifs for CREB-binding protein and Nfe2l2 transcription factors in the upstream enhancer of the mitochondrial uncoupling protein 1 gene. *J. Biol. Chem.* **277,** 34589–34600 (2002).

44. Kajimura, S. *et al.* Regulation of the brown and white fat gene programs through a PRDM16/CtBP transcriptional complex. *Genes Dev.* **22,** 1397–1409 (2008).

45. Ohno, H., Shinoda, K., Ohyama, K., Sharp, L. Z. & Kajimura, S. EHMT1 controls brown adipose cell fate and thermogenesis through the PRDM16 complex. *Nature* **504,** 163–167 (2013).

46. Seale, P. *et al.* Transcriptional control of brown fat determination by PRDM16. *Cell Metab.* **6,** 38–54 (2007).

47. Kajimura, S. *et al.* Initiation of myoblast to brown fat switch by a PRDM16-C/EBP-beta transcriptional complex. *Nature* **460,** 1154–1158 (2009).

48. Cohen, P. *et al.* Ablation of PRDM16 and beige adipose causes metabolic dysfunction and a subcutaneous to visceral fat switch. *Cell* **156,** 304–316 (2014).

49. Harms, M. J. *et al.* Prdm16 Is Required for the Maintenance of Brown Adipocyte Identity and Function in Adult Mice. *Cell Metab.* **19,** 593–604 (2014).

50. Rajakumari, S. *et al.* EBF2 Determines and Maintains Brown Adipocyte Identity. *Cell Metab.* **17,** 562–574 (2013).

51. Wang, W. *et al.* Ebf2 is a selective marker of brown and beige adipogenic precursor cells. *Proc. Natl. Acad. Sci. U. S. A.* **111,** 14466–14471 (2014).

52. Lowell, B. B. & Spiegelman, B. M. Towards a molecular understanding of adaptive thermogenesis. *Nature* **404,** 652–660 (2000).

53. Puigserver, P. *et al.* A cold-inducible coactivator of nuclear receptors linked to adaptive thermogenesis. *Cell* **92,** 829–839 (1998).

54. Kleiner, S. *et al.* Development of insulin resistance in mice lacking PGC-1α in adipose tissues. *Proc. Natl. Acad. Sci.* **109,** 9635–9640 (2012).

55. Lin, J. *et al.* Defects in Adaptive Energy Metabolism with CNS-Linked Hyperactivity in PGC-1α Null Mice. *Cell* **119,** 121–135 (2004).

56. Kong, X. *et al.* IRF4 is a key thermogenic transcriptional partner of PGC-1α. *Cell* **158,** 69–83 (2014).

57. Eguchi, J. *et al.* Interferon-regulatory factors (IRFs) are transcriptional regulators of adipogenesis. *Cell Metab.* **7,** 86–94 (2008).

58. Dempersmier, J. *et al.* Cold-Inducible Zfp516 Activates UCP1 Transcription to Promote Browning of White Fat and Development of Brown Fat. *Mol. Cell* (2015). doi:10.1016/j.molcel.2014.12.005

59. Tseng, Y.-H. *et al.* New role of bone morphogenetic protein 7 in brown adipogenesis and energy expenditure. *Nature* **454,** 1000–1004 (2008).

60. Contreras, C. *et al.* The brain and brown fat. *Ann. Med.* 1–19 (2014). doi:10.3109/07853890.2014.919727

61. Harms, M. & Seale, P. Brown and beige fat: development, function and therapeutic potential. *Nat. Med.* **19,** 1252–1263 (2013).

62. Gnad, T. *et al.* Adenosine activates brown adipose tissue and recruits beige adipocytes via A2A receptors. *Nature* **516,** 395–399 (2014).

63. Wang, G.-X. *et al.* The brown fat-enriched secreted factor Nrg4 preserves metabolic homeostasis through attenuation of hepatic lipogenesis. *Nat. Med.* **20,** 1436–1443 (2014).

Chapter 2:

# Cold–inducible Zfp516 Activates UCP1 Transcription to Promote Browning of White Fat and Development of Brown Fat

**Cold–inducible Zfp516 Activates UCP1 Transcription to Promote Browning of White Fat and Development of Brown Fat**


## Abstract

**Uncoupling protein 1 (UCP1) mediates non-shivering thermogenesis and, upon cold exposure, is induced in BAT and subcutaneous white adipose tissue (iWAT). Here, by high-throughput screening using the UCP1 promoter, we identify Zfp516 as a novel transcriptional activator of UCP1 as well as PGC1α thereby promoting a BAT program. Zfp516 itself is induced by cold and sympathetic stimulation through the cAMP-CREB/ATF2 pathway. Zfp516 directly binds to the proximal region of the UCP1 promoter, not to the enhancer region where other transcription factors bind, and interacts with PRDM16 to activate the UCP1 promoter. Although ablation of Zfp516 causes embryonic lethality, knockout embryos still show drastically reduced BAT mass. Overexpression of Zfp516 in adipose tissue promotes browning of iWAT even at room temperature, increasing body temperature, energy expenditure, and preventing diet-induced obesity. Zfp516 may represent a future target for obesity therapeutics.**


## INTRODUCTION

Whereas white adipose tissue (WAT) is the primary energy storage organ, brown adipose tissue (BAT) is specialized to perform nonshivering thermogenesis to maintain body temperature in mammals. Although the contribution of white fat to thermogenesis is not fully understood, inguinal WAT (iWAT) but not visceral WAT can undergo browning upon acute cold exposure. Nonshivering thermogenesis requires uncoupling protein-1 (UCP1), which dissipates the mitochondrial proton gradient to produce heat rather than ATP. Recently, metabolically relevant amounts of functional BAT or BAT-like tissue have been shown to be present in adult humans [1–4]. This finding has generated considerable interest as an increase in BAT activity in mice has been shown to have anti-obesity and anti-diabetic effects [5,6].

Lineage-tracing has shown that brown adipocytes may arise from $Myf5^+$/Sca-$1^+$/$Pax7^+$ cells of the dermomyotome, progenitors of skeletal muscle, cartilage, and dermis [7–10]. In addition to BAT, upon cold exposure, brown adipocyte-like cells termed "brite" or "beige" cells, which originate from $Myf5^-$ cells, may arise in inguinal WAT (iWAT) depots or there may be interconversion between white and brown adipocytes [11,12]. Contrary to classic BAT cells, brown adipocyte-like cells express very low levels of UCP1 and other BAT-enriched genes in non-stimulated conditions and are induced greatly following cold exposure [12,13]. As the thermogenic program in classic BAT and

emergence of brown adipocyte-like cells in iWAT are both induced by cold, a common regulatory mechanism may operate.

For transcriptional activation of UCP1, several transcription factors and coregulators, including PPARs, PGC1α, and ATF2, have been implicated, but are found in both WAT and BAT as well as in other tissues [14,15]. These factors have been shown to act through the well-characterized enhancer element located 2.5kb upstream of the UCP1 gene. In this regard, brown fat specific expression of UCP1 *in vivo* has been demonstrated by using a construct that contained the UCP1 proximal promoter region as well as the enhancer region [16]. Therefore, a yet to be identified cold inducible transcription factor(s) may bind the proximal promoter region to participate in activating UCP1 and other thermogenic genes.

Here, by performing high throughput screening of putative transcription factors for activation of the UCP1 promoter, we report that Zfp516, a novel, cold inducible transcription factor enriched in BAT compared to WAT, binds to the promoter region of UCP1. Zfp516 directly interacts with PRDM16 for transcriptional activation of thermogenic genes. Whereas ablation of Zfp516 causes embryonic lethality with drastically diminished BAT, overexpression of Zfp516 in adipose tissue causes browning of iWAT, increasing body temperature and energy expenditure to prevent diet induced obesity.

## RESULTS

To identify potential transcriptional activators of the UCP1 gene, we screened over 1100 transcription factor expression vectors representing two-thirds of known or putative transcription factors [17]. These expression vectors were individually cotransfected with a GFP reporter driven by the -5.5kb UCP1 promoter. Previous studies have shown that the -4.55kb promoter region to be sufficient for BAT-specific and regulated expression in transgenic mice [18]. Positive clones, identified by the detection of GFP signal, were subjected to a secondary screen employing luciferase instead of GFP as a reporter to quantitate promoter activation. During screening, known transcriptional activators of UCP1 that are widely expressed, such as CREB and ATF2, were identified as positives demonstrating the effectiveness of our screening. We identified 18 candidate genes independently capable of activating the UCP1 promoter more than 3-fold. We further selected those that were expressed at higher levels in BAT compared to WAT by RT-qPCR (Figure 3). Here, we studied one of the best candidates, the previously uncharacterized Krüppel-like zinc finger transcription factor, Zfp516 (Gene ID: 329003), for its role in the transcriptional regulation of UCP1.

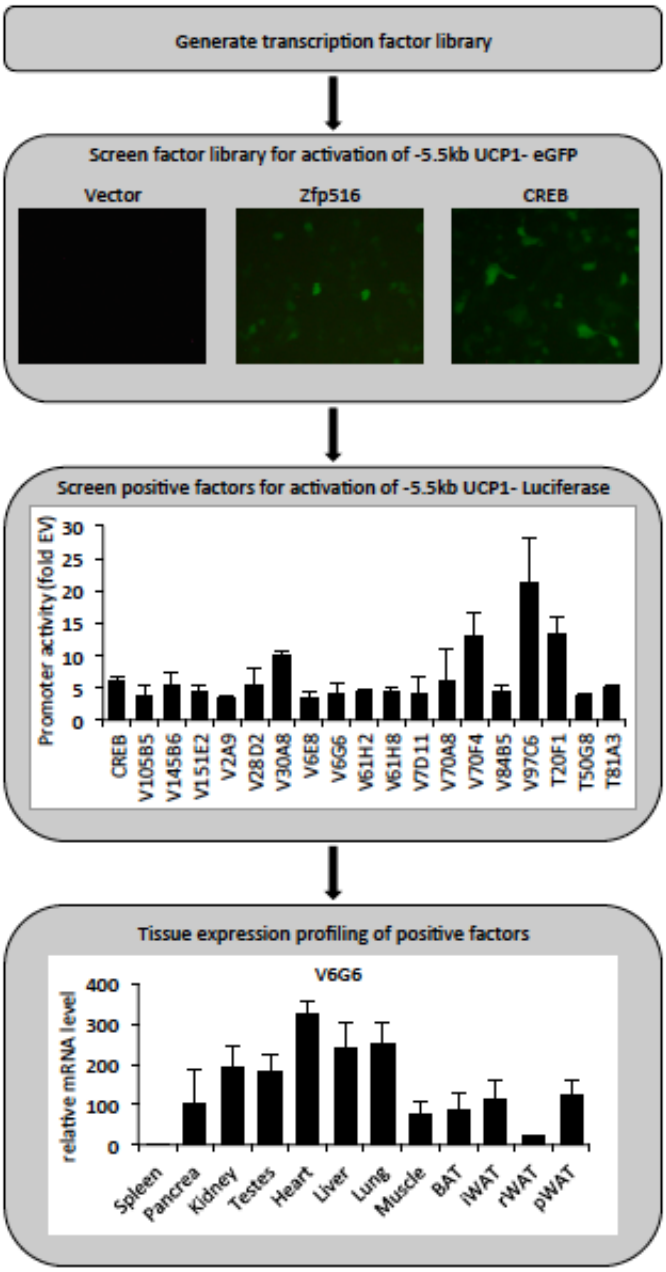


**Figure 3: Schematic representation of the screening of transcription factors for activation of the UCP1 promoter.** Top, 293FT cells were transfected with -5.5kB UCP1-eGFP and the indicated vectors. GFP fluorescence was assessed 48 hours post transfection. Middle, 293FT cells were transfected with -5.5kB UCP1-Luc and the indicated vectors and assayed at 48 hours post transfection. Positives from screening effort are shown (n=4). Bottom, RT-qPCR for V6G6 from the indicated tissues from C57BL/6 mice. For screening purposes, this is an example of a negative gene (n=3). Data shown are mean +/- SEM.

**Zfp516 directly binds and activates UCP1 promoter**

As Zfp516 activity or function has not been studied previously, we performed a motif analysis of Zfp516, which identified ten C2H2-type zinc fingers, widespread DNA binding motifs of eukaryotic transcription factors (Fig. 4A top) [19]. Cell fractionation experiments to examine the localization of Zfp516 in the brown preadipocyte cell line, HIB-1B, showed that Zfp516 was present exclusively in the nucleus (Fig. 4A bottom). As detected in the initial screening, we established that Zfp516 robustly activated the UCP1 promoter-GFP reporter (Fig. 4B top). As compared to empty vector control, cotransfection of Zfp516 with the -5.5kb UCP1 promoter-luciferase resulted in a 4-fold activation of the UCP1 promoter (Fig. 4B bottom). This degree of UCP1 promoter activation was similar to that observed by cotransfection of CREB. We found that by both RT-qPCR and immunoblotting Zfp516 was enriched in BAT in comparison to WAT depots (Fig. 4C top). When BAT was fractionated into adipocytes

and stromal vascular fraction (SVF) that contain brown preadipocytes, as expected, we detected UCP1 expression to be 30-fold higher in adipocytes than SVF. We found that Zfp516 expression was 6-fold higher in adipocytes compared to SVF (Fig. 4C bottom).

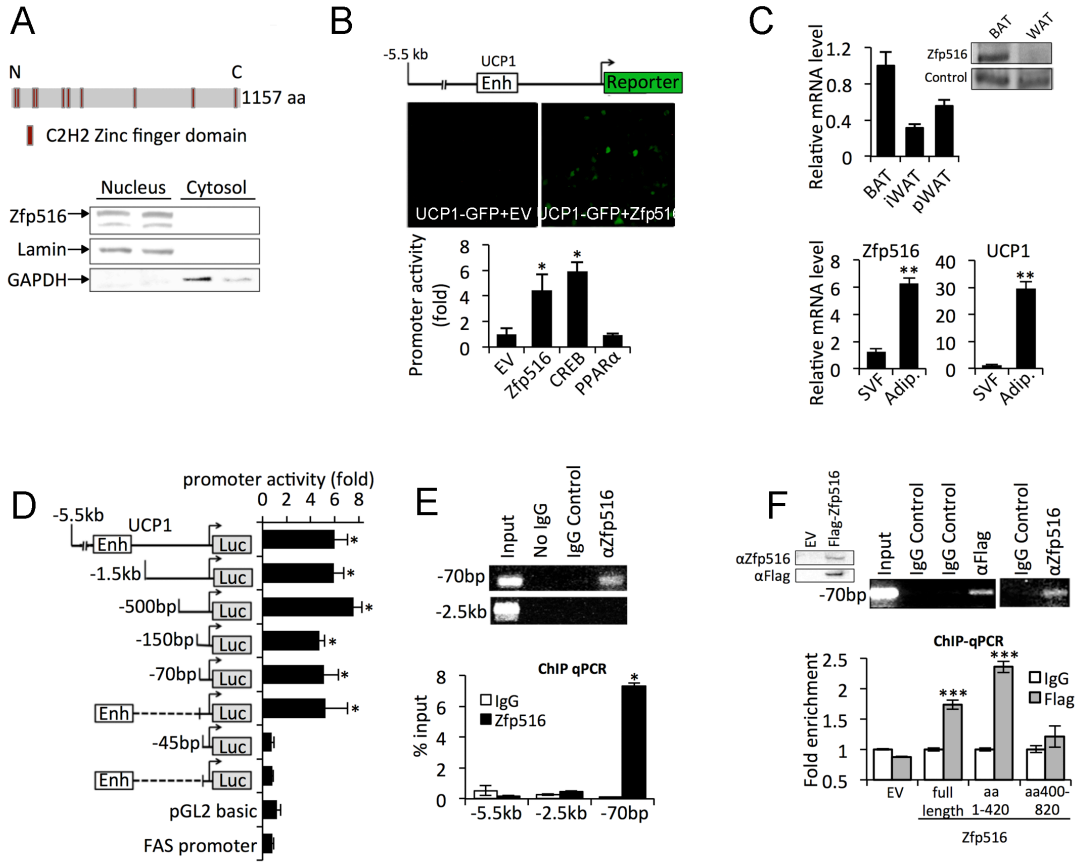


**Figure 4. Zfp516 is a Brown Fat- Enriched Transcription Factor that binds and activates UCP1 promoter.** A. Top, diagram of Zfp516 structure. Bottom, immunoblotting for Zfp516, lamin (nuclear), and GAPDH (cytosolic) in nuclear and cytosolic fractions of HIB-1B cells. B. Top, GFP fluorescence of 293FT cells transfected with -5.5kb UCP1-GFP and either empty vector (EV) or Zfp516. Bottom, relative luciferase activity of 293FT cells cotransfected with -5.5kb UCP1-Luc and the indicated expression vector. C. Top and inlay, RT-qPCR and immunoblotting for Zfp516 mRNA and protein levels in BAT and WAT tissues from 6 week-old C57BL/6 mice (n=4 mice). Bottom, RT-qPCR for Zfp516 and UCP1 mRNA levels in the adipocyte fraction and SVF from BAT. D. Schematic representation of 5' deletion constructs of the UCP1 promoter-luciferase and relative luciferase activity in 293FT cells cotransfected with indicated promoter construct and Zfp516 (expressed as fold of vector control). E. Top, ChIP for Zfp516 association to the UCP1 promoter in BAT. Bottom, qPCR for the ChIP DNA for Zfp516 association to the UCP1 promoter in BAT. F. Top-left, immunoblotting of lysates from 293FT cells transfected with -5.5kb UCP1-GFP with Flag-Zfp516 or vector. Top-right, ChIP for Flag-Zfp516 association to the UCP1 promoter using both αFlag and αZfp516 antibodies. Bottom, qPCR quantification of ChIP DNA for the association of full length Zfp516 or truncations of Zfp516 to the UCP1 promoter in 293FT cells. See also Figure S1, S2, and S3. Error bars are +/- SEM. *p<0.05; **p<0.01; ***p<0.001

To start defining how Zfp516 activates the UCP1 promoter, 5' deletions of the UCP1 promoter driving a luciferase reporter were generated and cotransfected along with Zfp516 into 293FT cells. Contrary to the majority of known transcriptional activators of UCP1 that act at the enhancer element at -2.5kb upstream of the transcription start site [20,21], activation of the UCP1 promoter by Zfp516 was maintained even after deletion of the -2.5kb enhancer element. Further, all UCP1 promoter constructs deleted down to -70bp showed over 4.5-fold activation upon Zfp516 cotransfection. However, UCP1 promoter activation by Zfp516 was lost when the promoter was deleted to -45bp indicating that Zfp516 worked through the sequence from -70 to -45bp. Linking the -2.5kb UCP1 enhancer element to the -70bp to -45bp sequence did not show any further effect (Fig. 4D). Gel mobility shift assay showed a complex formation between Zfp516 and -70 to -45bp sequence, which could be supershifted by Zfp516 antibodies (Fig. 5A). Chromatin immunoprecipitation (ChIP) of interscapular BAT from C57BL/6 mice showed clear evidence of Zfp516 binding to the proximal UCP1 promoter region *in vivo* (Fig. 4E). We conclude that Zfp516 functions through the sequence from -70 to -45bp.

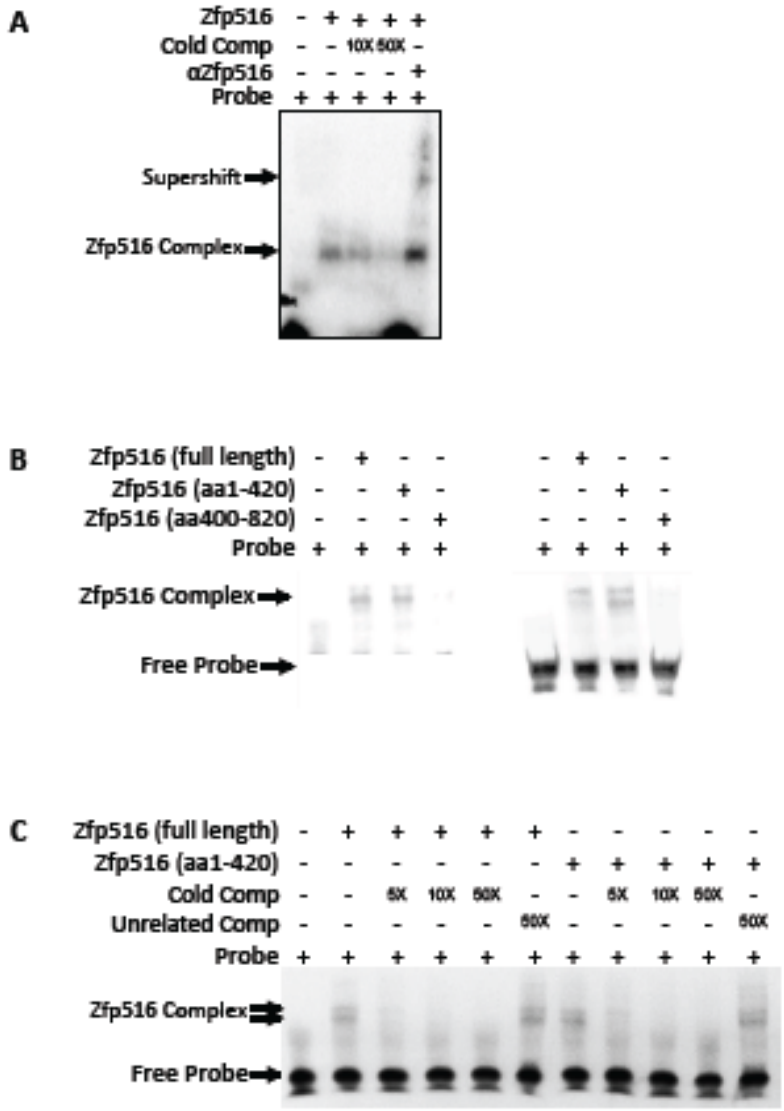


**Figure 5. Zfp516 binds to the proximal UCP1 promoter.** A. Gel shift assay was performed with nuclear extracts of 293FT cells transfected with flag-Zfp516. Each reaction contained 0.1 µg of poly(dI-dC), 1 mM DTT, 0.1 ng of 32P-labeled oligonucleotide probe. Cold probe or 1µg of αZfp516 were added as indicated. B. Gel shift assay was performed with nuclear extracts of 293FT cells transfected with either the full length Zfp516 or truncations aa1-420 or aa400-820. Each reaction contained 12pmol of biotin labelled probe, 0.1µg of poly(dI-dC) and 1 mM DTT. 2 independent experiments are shown. C. Gel shift assays as in B with cold probe and unrelated probe as competitors.

As indicated in Fig.1A, Zfp516 contains 10 Zinc fingers primarily at the N-terminus. Therefore in addition to full length, we generated truncations of Zfp516 containing either the first one third (AA1-420) (7 Zinc fingers) or second third (AA400-820) (2 Zinc fingers) to use in ChIP assays. As expected, use of the antibody showed the binding of full length Zfp516 at the proximal UCP1 promoter region. ChIP using Zfp516 antibody showed the same results (Fig. 4F top). ChIP qPCR showed that in addition to full length Zfp516, the first one third of the N-terminus (AA1-420) but not the second third (AA400-820) showed binding to the UCP1 promoter indicating that Zfp516 interacted with UCP1 promoter through the first third from the N-terminus (Fig. 4F bottom). Similarly, gel shift assay showed that full-length Zfp516 and Zfp516 (AA1-420) but not Zfp516 (AA400-820) form DNA-protein complexes (Fig. 5 B,C). These data indicate that Zfp516, through its N-terminal domain binds to the UCP1 promoter region from -70 to -45bp to activate transcription.

In addition to UCP1, we also examined several BAT-enriched gene promoters for sequence similarity to -70 to -45bp of UCP1 promoter. Indeed several of BAT-enriched genes contained the DNA sequence, CCACT, present in the UCP1 promoter. We chose PGC1α and Cox8b, which contained sequences with the highest alignment score, for further examination. ChIP analysis of the 293FT cells transfected with Zfp516 and the PGC1α or Cox8b promoter-reporters showed that, indeed, Zfp516 was bound to the -2.4kb region of the PGC1α promoter and -2.8kb region of Cox8b promoter. Cotransfection of Zfp516 with the -2.4kb PGC1α promoter-luciferase construct in 293FT cells resulted in a 15-fold activation of the PGC1α promoter (Fig. 6). These results show that Zfp516 binds and activates not only UCP1 but other BAT gene promoters as well.

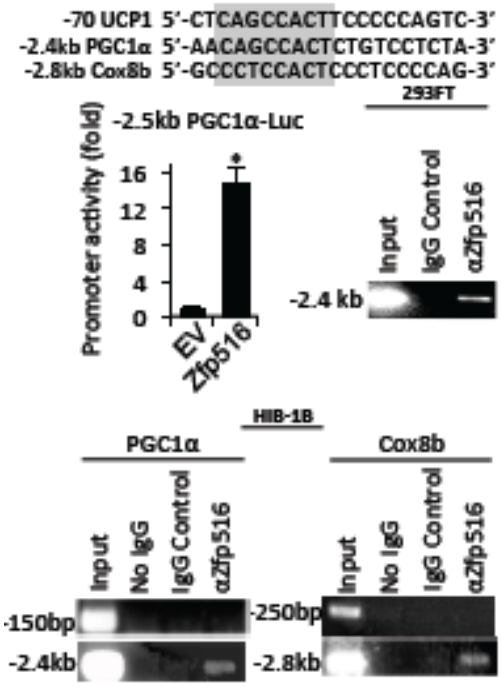


**Figure 6. Zfp516 binds to PGC1α and Cox8b promoters for activation.** Top, sequence alignment of identified Zfp516 cis element in the UCP1 promoter to select regions of other BAT promoters with highlighted putative Zfp516 response element. Middle-left, relative luciferase activity of 293FT cells transfected with -2.5kb PGC1α- Luc with Zfp516 or vector control (n=6). Data shown are mean +/- SEM. Middle-right, ChIP for Zfp516 association to the PGC1α promoter in 293FT cells cotransfected with -2.5kb PGC1α-Luc and Zfp516 or vector control. Bottom-left, ChIP for Zfp516 association to the PGC1α promoter in HIB-1B cells. Bottom-right, ChIP for Zfp516 association to the Cox8b promoter in HIB-1B cells. Values are mean ± SEM and are normalized to the empty vector control. *$p<0.05$; **$p<0.01$.

**Zfp516 interacts with PRDM16**

Next we asked whether Zfp516 interacts with known transcription factors or cofactors that have been reported to be involved in UCP1 activation. PGC1α, PPARγ, C/EBPβ, and PRDM16 were cotransfected with Zfp516 and immunoprecipitated with the Zfp516 antibody. Immunoblotting with antibodies against these transcription factors identified PRDM16, but not other factors, as an interacting partner of Zfp516 (Fig. 7A top-left). Interaction between Zfp516 and PRDM16 was confirmed by using Flag-tagged Zfp516 and V5-tagged PRDM16 as well as using endogenous proteins from mouse BAT (Fig. 7A top-right, bottom-left). Use of various GST-PRDM16 fusion proteins indicated that Zfp516 can directly interact with PRDM16 AA881-1038, a region shown to interact with other transcription factors [22] (Fig. 7A bottom-right).

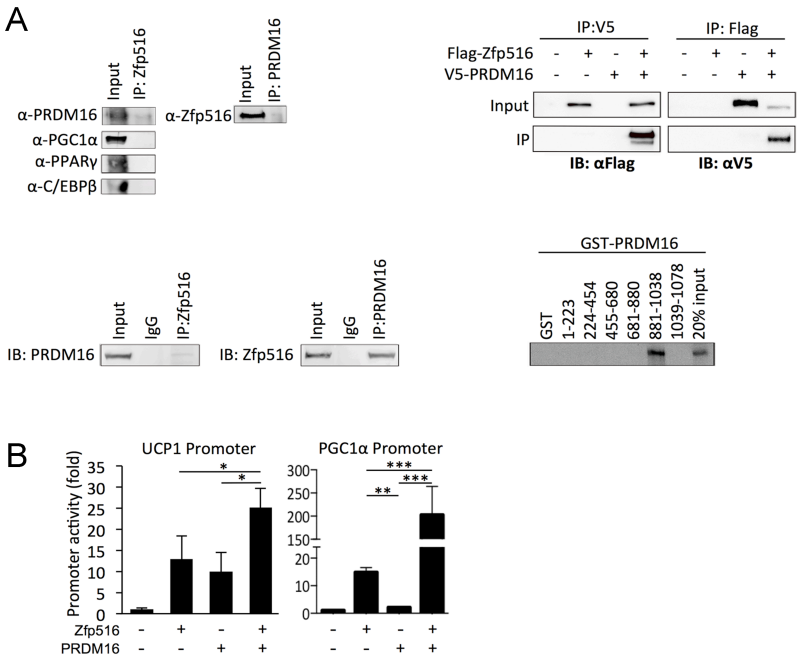


**Figure 7. Zfp516 directly interacts with PRDM16.** A. Top-left (left column), immunoblot for various brown fat specific transcription factors after IP with αZfp516 antibody in 293FT cells cotransfected with Zfp516 and the indicated TF. Top-left (right side), immunoblot for Zfp516 protein after IP with αPRDM16 of lysates coexpressing Zfp516 and PRDM16. Top-right, immunoblot with αV5 or αFlag after IP with either Flag or V5 respectively of 293FT lysates transfected the indicated vectors. Bottom-left, immunoblot for either Zfp516 or PRDM16 after IP with indicated antibody of 50μg of BAT nuclear extracts. Bottom-right, Autoradiograph of GST pulldown using GST fusion proteins containing the indicated domains of PRDM16 and $^{35}$S-labelled *in vitro* translated Zfp516. B. Left, luciferase activity of 293FT cells cotransfected with the -5.5kb UCP1 promoter with Zfp516 and PRDM16 either together or separately. Right, luciferase activity of 293 FT cells cotransfected with the -2.4kb PGC1α promoter with Zfp516 and PRDM16 either together or separately. Error bars are +/- SEM. *p<0.05; **p<0.01; ***p<0.001

To examine the functional significance of Zfp516 and PRDM16 interaction in the activation of UCP1 and other BAT-enriched genes, we cotransfected Zfp516 and PRDM16 with the -5.5kb UCP1-luciferase reporter construct. Zfp516 and PRDM16 individually activated the UCP1 promoter 13- and 10- fold, respectively while, cotransfection of both resulted in a 25-fold activation (Fig. 7B left). Cotransfection of Zfp516 and PRDM16 together with the PGC1α promoter caused a robust 200-fold increase in promoter activity whereas Zfp516 and PRDM16 individually activated the PGC1α promoter 15- and 3-fold respectively (Fig. 7B right). These data show that Zfp516 and PRDM16, upon their interaction, further activate transcription of BAT genes. Since the DNA binding activity of PRDM16 is not required for BAT gene induction, Zfp516 may recruit PRDM16 to the promoter regions of BAT-enriched genes. In this regard, Re-Chip indicated that Zfp516 and PRDM16 were bound to the UCP1 promoter in a similar region (data not shown).

**Zfp516 is cold induced via cAMP-CREB/ATF pathway**

Expression of many BAT-enriched genes as well as BAT development are known to be induced by cold [23–26]. Therefore, we next assessed possible regulation by the β-adrenergic receptor-cAMP pathway of Zfp516 itself. We treated HIB-1B cells with IBMX, Isoproterenol, or Forskolin, agents that can increase intracellular cAMP levels. Treatment of cells with the β-adrenergic agonist, isoproterenol resulted in approximately 2-fold increase in both Zfp516 and UCP1 mRNA levels. Other known cold responsive genes such as PGC1α and Dio2 were also induced while PRDM16 remained unchanged (Fig. 8A top-left). Treatment of HIB-1B cells with IBMX, a phosphodiesterase inhibitor, resulted in a rapid increase in Zfp516 mRNA level reaching maximal increase of 2-fold after 6h treatment which was maintained up to 24h. Expression of other known targets such as UCP1 and PGC1α showed similar pattern during IBMX treatment but increased by 13- and 2-fold, respectively (Fig. 8A top-right). Treatment with these agents resulted in increased Zfp516 protein levels in all treatment conditions (Fig. 8A bottom). We next generated a reporter construct linking -2.0kb of the Zfp516 promoter to a luciferase reporter and cotransfected it with CREB, ATF2, and other known BAT transcription factors. Motif search of the proximal -2.0kb of the Zfp516 promoter region revealed two half CREs at -1.1kb and -1.8kb upstream of the Zfp516 transcription start site. Indeed, cotransfection of CREB or ATF2 with the Zfp516 promoter-reporter construct increased the luciferase activity by 11- and 2-fold, respectively, whereas other transcription factors, such as PRDM16, C/EBPβ, PGC1α, PPARα, and PPARγ, did not show any effect (Fig. 8B). These data show that Zfp516 is induced via cAMP-CREB/ATF2 pathway.

To test cAMP pathway *in vivo* we treated mice with the β-adrenergic agonist, CL316,243 for 10d. Expression of UCP1 and Zfp516 was increased 1.5- to 2-fold, respectively in BAT (Fig. 8C). There was no change in UCP1 or Zfp516 expression levels in perigonadal WAT (pWAT), a visceral WAT depot. In contrast, in iWAT, UCP1 and Zfp516 were

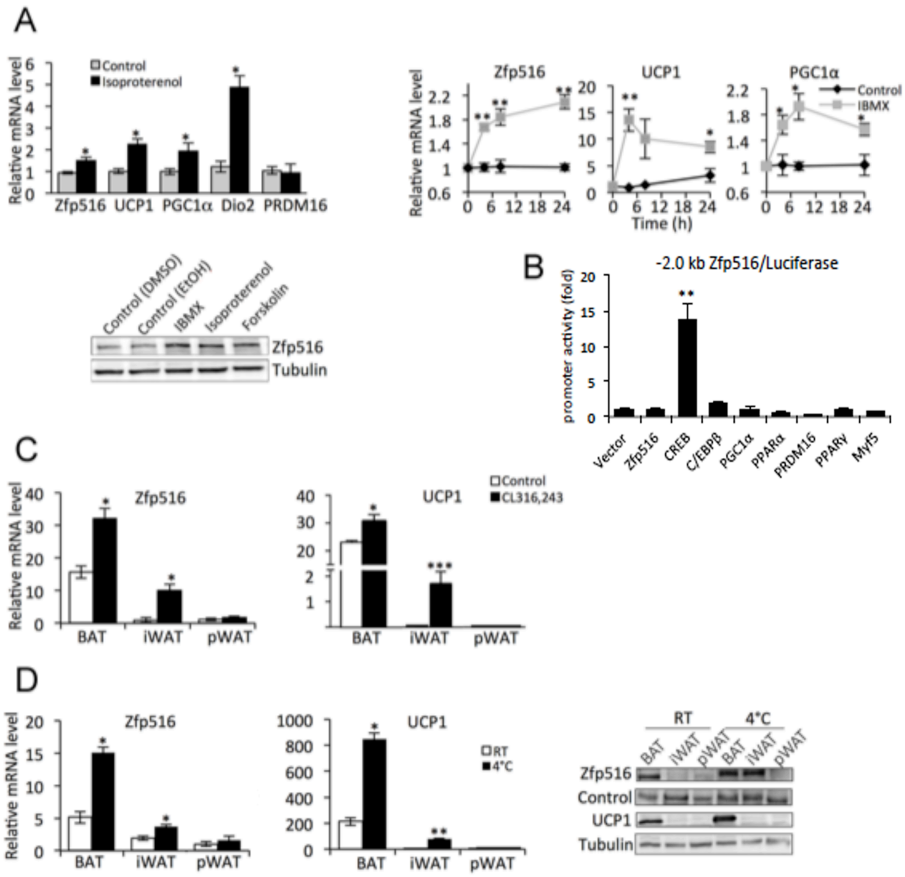


**Figure 8. Zfp516 is regulated by Cold through CREB/ATF.** A. Top-left, RT-qPCR for selected genes in HIB-1B cells with or without 4h treatment with 10μM isoproterenol. Top-right, RT-qPCR for Zfp516, UCP1, and PGC1α mRNA in HIB-1B cells during 500μM IBMX treatment. Bottom, immunoblotting for Zfp516 or tubulin in HIB-1B cells treated with vehicle or indicated compound for 12h. Values are normalized to nontreated cells. B. Relative luciferase activity of 293FT cells transfected with the -2.0kb Zfp516-Luc and indicated transcription factor expression vector. C. RT-qPCR for Zfp516 and UCP1 mRNA in various tissues of wild-type mice following 10d of intraperitoneal injection with either CL316,243 or saline. D. RT-qPCR for Zfp516 and UCP1 mRNA (left and center) and immunoblotting for indicated proteins (right) in various adipose depots of wild-type mice exposed to cold (4°C) for 6h. See also Figure S4. Error bars are +/- SEM. *p<0.05; **p<0.01; ***p<0.001

drastically increased by 30- and 10-fold, respectively (Fig. 8C). Overall, these results indicate that Zfp516 expression in iWAT, although its absolute levels are still lower than in BAT, is induced to a greater extent by β-adrenergic agonist treatment.

Next we subjected mice to a 6h cold challenge. Similarly to β-adrenergic agonist treatment, we detected an increase of UCP1 and Zfp516 mRNA and protein levels in BAT upon cold exposure. Zfp516 expression in pWAT was lower and remained low,

even after cold exposure. In iWAT, UCP1 and Zfp516 expression increased 40- and 2.5-fold, respectively, with Zfp516 expression approaching the expression levels detected in BAT at room temperature (Fig. 8D). Overall, we conclude that although Zfp516 level is higher in BAT than WAT, the degree of induction by β-agonist or cold exposure was much higher in iWAT compared to BAT while there was no change in pWAT. These data suggest that Zfp516 may be involved in the browning of iWAT.

**Zfp516 promotes browning of white adipose tissue**

Next, to test the effect of Zfp516 overexpression in adipose tissue *in vivo*, we generated transgenic mouse lines expressing Zfp516 driven by the -5.4kb aP2 promoter. Although endogenous Zfp516 expression is significantly higher in BAT than WAT (Fig. 4C), the fold increase of Zfp516 in iWAT and pWAT of transgenic mice was greater than in BAT (50-fold versus 10-fold) (Fig. 9A). Zfp516 expression in other tissues was unaffected (Fig. 10H). Similarly, Zfp516 protein levels were elevated in two independent transgenic lines in all adipose depots compared to wild-type mice. We then examined UCP1 levels by immunoblotting. UCP1 levels were increased approximately 3-4 fold in BAT of aP2-Zfp516 mice compared to wild-type littermates. Strikingly, although its level was lower than that in BAT, the fold increase of UCP1 was more drastic in iWAT, but not pWAT, of aP2-Zfp516 mice even in the absence of cold or adrenergic stimuli (Fig. 9B). Noticeably, iWAT of aP2-Zfp516 mice that were maintained at room temperature showed large clustered populations of cells with smaller multilocular lipid droplets, a characteristic of the browning of WAT depots whereas pWAT of aP2-Zfp516 mice showed no difference in morphology compared to wild-type littermates (Fig. 10A, 10B ). UCP1 immunostaining of UCP1 in iWAT sections from aP2-Zfp516 mice maintained at room temperature also showed robust UCP1 staining (Fig. 9B), while no significant staining was observed in wild type littermates.

To examine overall gene expression changes in iWAT, RNA from iWAT of wild-type and aP2-Zfp516 mice were subjected to Affymetrix microarray analysis. We found that transgenic expression of Zfp516 led to upregulation of a broad program of BAT-enriched genes while common adipocyte markers were not affected significantly (Fig. 9C left). RT-qPCR analysis of these samples showed that expression levels of BAT-enriched genes, such as UCP1, PGC1α, and Cox8b, were all significantly elevated in iWAT of aP2-Zfp516 mice, while PPARγ and PRDM16 remain unaffected (Fig. 9C top-right). Considering the striking increase in UCP1 levels as well as extensive browning of iWAT of aP2-Zfp516 mice, we next assessed the metabolic effect in the transgenic animals. We observed 10% higher oxygen consumption rate ($VO_2$) in transgenic mice during both day and night cycles (Fig. 9D). We next tested whether changes in respiratory activity in iWAT could contribute to the altered respiratory activity in these transgenic mice. Indeed, upon using a Seahorse XF-24 Extracellular flux analyser, we found a 70% increase in oxygen consumption rate (OCR) in iWAT of transgenic mice (Fig. 9E). We did not detect

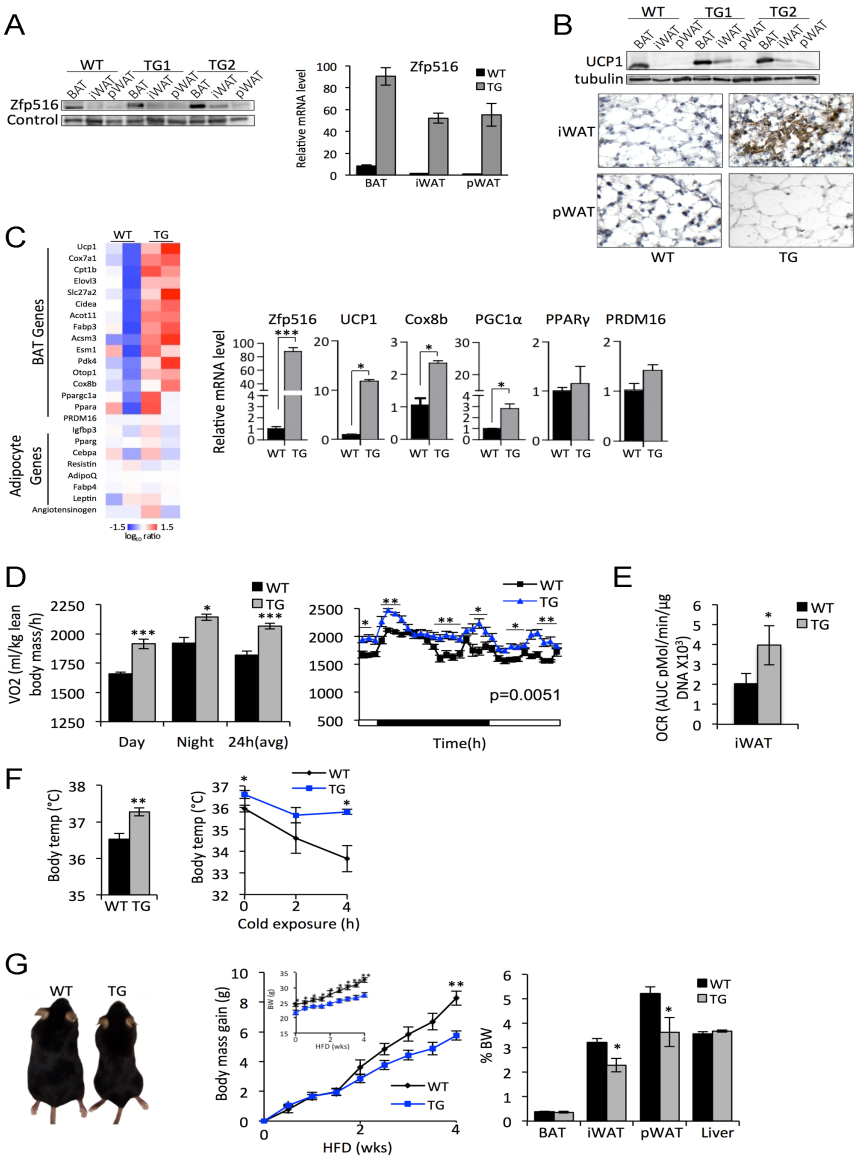


**Figure 9. Zfp516 Promotes Browning of White Adipose Tissue.** A. Left, immunoblotting for Zfp516 in adipose depots of WT and aP2-Zfp516 mice (TG) with different transgene copy number. Right, RT-qPCR for Zfp516. B. Top, immunoblotting for UCP1 in adipose depots of WT and TG mice. Bottom, immunostaining for UCP1 in sections of iWAT and pWAT from WT and TG mice. C. Left, microarray analysis from iWAT of WT or TG mice. Right, RT-qPCR of genes from microarray in WT or TG mice (n= 3 per group). D. $VO_2$ assayed by indirect calorimetry in WT and TG mice on chow diet (CD) (n=6 mice per group). E. Oxygen consumption rate of iWAT from WT or TG mice. F. Rectal temperature measured in 15wk old WT and TG mice fed CD at room temperature (left) and after 4 h cold exposure (right) (n=7-8 mice per group). G. Left, representative photograph of 26wk old WT or TG mice fed HFD for 16wk. Center, body mass gain for the mice from left. Inlay, body weight in WT and TG mice fed HFD starting at 6wk old (n=6-8 mice per group). Right, mass of each adipose tissue depot and liver represented in percentage of body weight in the mice mentioned above. See also Figure S5. Error bars are +/- SEM. *p<0.05; **p<0.01; ***p<0.001

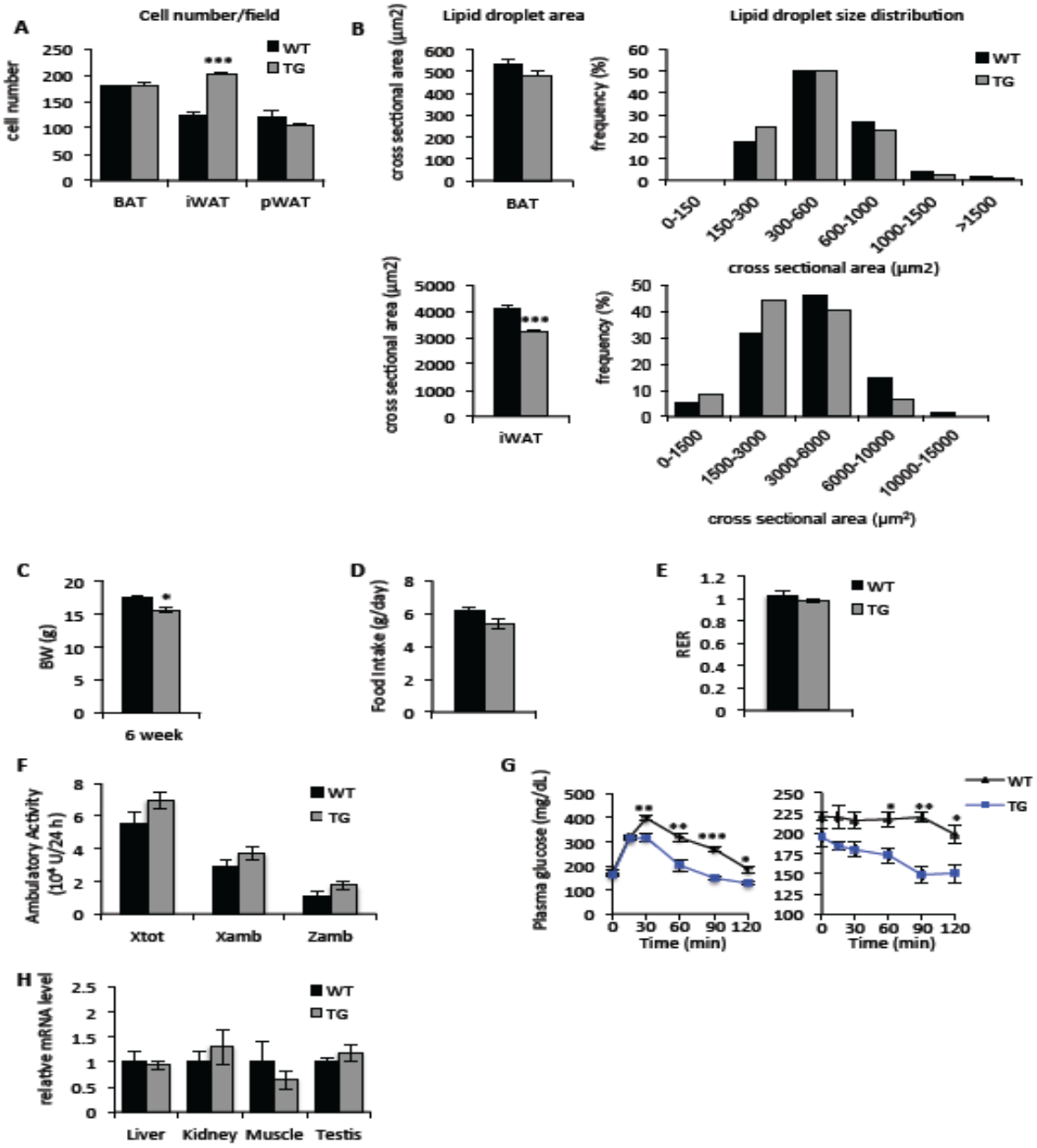


**Figure 10. Zfp516 Promotes Browning of Inguinal WAT**. A. Left, cell number/ field in BAT from WT or TG mice (n=3). B. Top, lipid droplet area and lipid droplet size distribution in BAT from WT or TG mice. Bottom. Lipid droplet area (center) and lipid droplet size distribution (right) in iWAT from WT or TG mice (n=3). C. Body weight of WT and TG mice on CD at 6 weeks of age (n=8 mice per group). D. Average food intake of WT and TG mice on CD at 6 weeks of age (n=8 per group). E. Resting energy rate of WT and TG mice on CD at 6 week of age (n=8 per group). F. activity assayed by indirect calorimetry in WT and TG mice on CD (n=8 mice per group). G. Glucose tolerance (left) and Insulin tolerance test (right) in 10 week old mice after 4 weeks of HFD. (n=8-10). H. RT-qPCR for Zfp516 in indicated tissues from 10 week-old WT or aP2-Zfp516 mice (n=3). *p<0.05; **p<0.01; ***p<0.001 .

significant alterations of OCR in BAT of transgenic mice (data not shown). Strikingly, aP2-Zfp516 mice fed a standard chow diet and maintained at room temperature had 0.7°C higher core body temperature than their wild-type littermates, although its implication in thermogenesis is not clear [27] (Fig. 9F). However, when subjected to an acute cold exposure, these transgenic mice showed rectal temperature to be dropped by 1°C after 4h at 4°C whereas the wild-type mice showed drop of 3°C, showing improved thermogenic capacity in Zfp516 transgenic mice. Taken together, these data show that Zfp516 overexpression causes browning of iWAT that results in increase in oxygen consumption and increased cold resistance.

We next subjected aP2-Zfp516 transgenic mice to high-fat diet (HFD) to test whether the increase in thermogenesis results in protection from diet-induced obesity. Interestingly, aP2-Zfp516 transgenic mice have significantly smaller body weight compared to wild type littermates on chow diet at room temperature, despite no change in food intake or activity level in these mice (Fig.10 C-F). When subjected to HFD feeding, aP2-Zfp516 transgenic mice gained 30% less weight than their wild-type littermates (Fig. 9G). Noticeably, the iWAT and pWAT depots of transgenic mice had approximately 30% lower weights than wild-type littermates, even when normalized to body weight while BAT as well as other organs such as liver was unaffected (Fig. 9G right). These data suggest that Zfp516 overexpressing mice are protected from diet induced obesity. After 4wks on HFD, mice were subjected to glucose and insulin tolerance tests. We found that Zfp516 transgenic mice had improved glucose tolerance and insulin sensitivity as compared to wild-type littermates (Fig. 10G). Taken together, these data show that overexpression of Zfp516 causes an increase in UCP1 and browning of iWAT resulting in increased energy expenditure, improved cold tolerance, as well as protection against diet-induced obesity.

**Ablation of Zfp516 impairs BAT development *in vivo***

To further examine Zfp516 function in BAT program *in vivo*, we ablated Zfp516 in mice by using embryonic stem cells containing a gene trap inserted in intron 1 of the Zfp516 gene (Fig. 11B). Mice homozygous for the Zfp516 gene-trap were found to die immediately after birth due to a yet to be defined role of this gene during development. Therefore, we examined Zfp516$^{-/-}$ embryos at E20.5 when the presence of BAT, but not WAT, can be easily detected in wild-type mice. RT-qPCR showed that Zfp516 expression was undetectable in Zfp516$^{-/-}$ embryos compared to wild-type littermates confirming Zfp516 ablation (Fig. 11C). Although Zfp516$^{-/-}$ embryos were somewhat smaller at E17.5, they were visibly indistinguishable from their wild-type littermates in terms of size at E20.5, yet the defective BAT formation was easily detected (Fig. 12A). UCP1 staining on transverse sections of embryos showed a complete absence of UCP1 in the Zfp516$^{-/-}$ presumptive BAT (Fig. 12B top). Haematoxylin and eosin (H&E) staining of the WAT/BAT boundary indicated abnormal cell morphology in the presumptive BAT

of Zfp516 deficient embryos, while nearby WAT showed decreased cell size (Fig. 12B upper-middle). Oil Red O staining of presumptive BAT from Zfp516$^{-/-}$ embryos revealed a near complete loss of lipid staining (Fig. 12B lower-middle). Furthermore, transmission electron microscopy revealed that mitochondria from presumptive BAT from Zfp516$^{-/-}$ embryos have randomly-oriented cristae as compared to the classic laminar cristae found in wild-type littermates (Fig. 12B bottom).

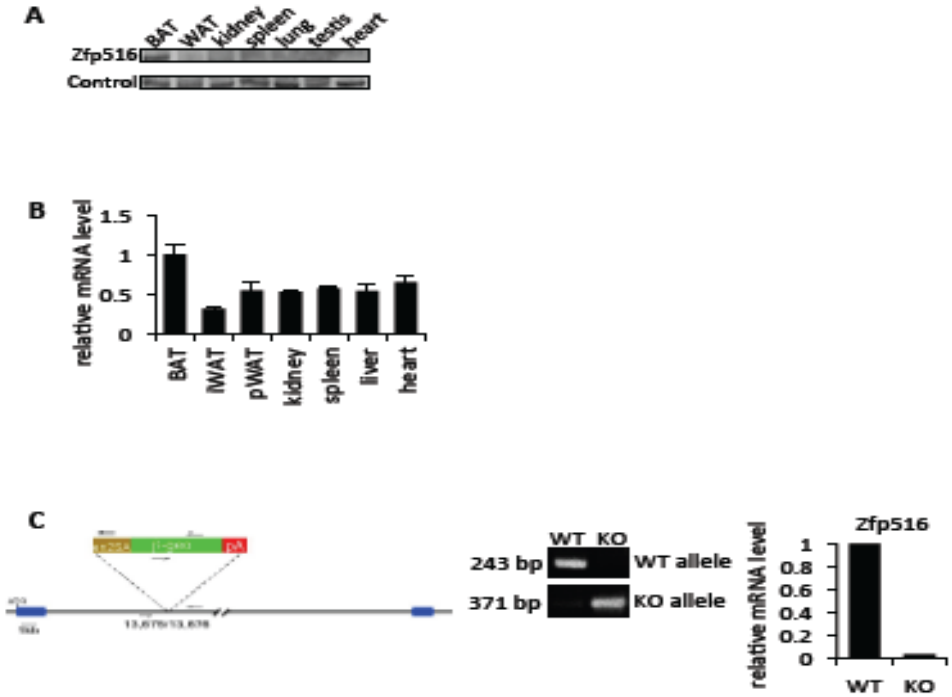


**Figure 11. Generation of Zfp516 knockout mice**. A. Immunoblotting for Zfp516 in the indicated tissues of WT mice. B. RT-qPCR for Zfp516 in the indicated tissues. n=3. C. Left, schematic representation of gene trap insert in Intron 1 of Zfp516 with genotyping primer orientation. Center, representative genotyping gel delineating WT and KO allele. Right, RT-qPCR for Zfp516 mRNA in WT and KO BAT (n=4). Data shown are mean +/- SEM.

We next examined gene expression in presumptive BAT of our Zfp516 ablated embryos at the global level by performing Affymetrix microarray analysis. Clustering of significantly affected genes into functionally related gene groups revealed down regulation of a broad program of genes required for BAT function, whereas expression of muscle genes were elevated (Fig. 12C). Common adipocyte markers were not significantly altered (data not shown). The gene expression analysis of BAT from Zfp516$^{-/-}$ embryos by RT-qPCR revealed that expression of BAT-enriched genes, such as UCP1, PRDM16, PGC1α, PPARα, C/EBPβ, Elovl3, and FoxC2, was all significantly lower by 40-85% (Fig. 12D left). In contrast, myogenic genes, such as MyoD, MyoG, Mck, Myf5, and Myf6, were significantly upregulated by 3- to 14-fold (Fig. 12D right).

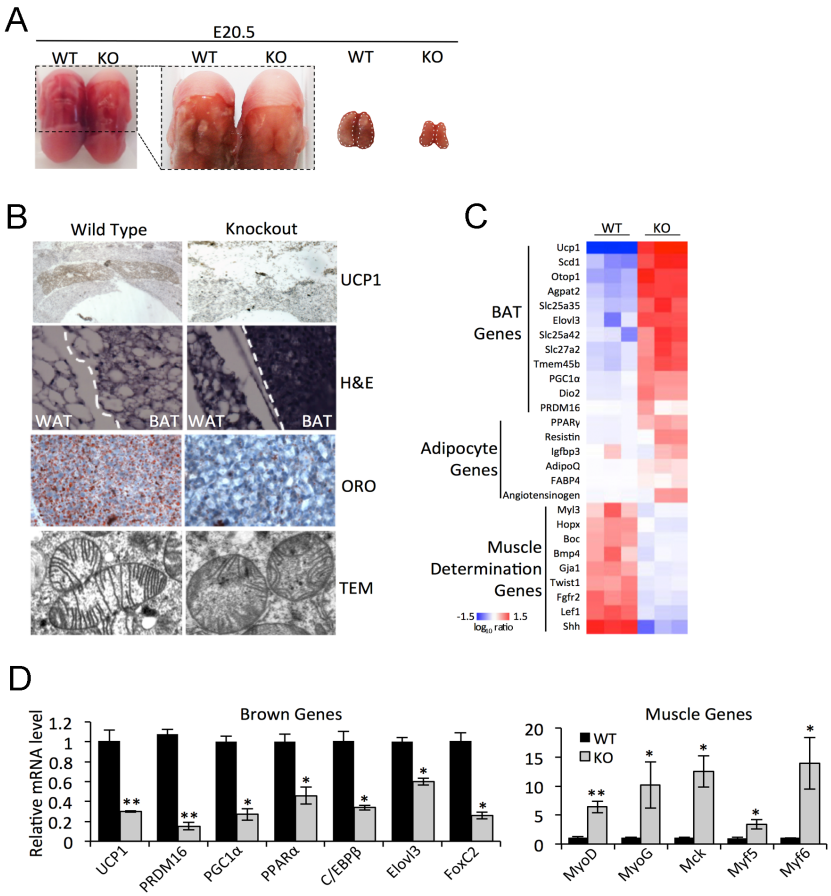


**Figure 12. Zfp516 ablation blocks brown fat development in mice.** A. Left, E20.5 WT and Zfp516 KO embryos from back view. White dots delineate area of BAT or presumptive BAT. Right, cropped image from left. B. Top, immunostaining for UCP1 in BAT or presumptive BAT in WT and KO embryos. Top middle, H&E staining of the BAT/WAT border in WT and KO mice. Bottom middle, ORO staining of WT or KO BAT. Bottom, transmission electron microscopy of WT and KO BAT mitochondria. C. Microarray analysis from BAT or presumptive BAT of WT or KO E20.5 embryos. D. RT-qPCR for BAT enriched (left) and muscle (right) genes in BAT from E17.5 WT or KO embryos (n=3). See also Figure S6. Error bars are +/- SEM. *p<0.05; **p<0.01; ***p<0.001.

We conclude that Zfp516 ablation abrogates the induction of UCP1 and other BAT genes during normal BAT development.

**Zfp516 promotes brown adipogenesis and suppresses myogenesis *in vitro***

As stated above, BAT develops from Myf5$^{+}$ precursors that can differentiate to both muscle and BAT. Since we detected an increase in myogenic genes accompanied by decrease in BAT enriched genes in presumptive BAT of Zfp516$^{-/-}$ embryos, we employed C2C12 cells to test the ability of Zfp516 to induce UCP1 and other thermogenic genes to promote brown adipocyte differentiation. C2C12 cells were transduced with adenovirus

expressing Zfp516 and treated with brown adipogenic cocktail. Endogenous expression of Zfp516 in C2C12 was very low but was substantially increased by adenoviral infection as verified at the protein level by immunoblotting (Fig. 13A top-left) and at the mRNA level by RT-qPCR (data not shown). Upon infection with Zfp516, we observed an activation of the brown adipogenic program in C2C12 cells as evidenced by enhanced lipid accumulation (Fig. 13A top-center) and increased expression of UCP1 and Cox8b (respectively by 4- and 2- fold; Fig. 13A top-right). In contrast, in myogenic conditions, Zfp516-overexpressing cells failed to undergo efficient myogenic differentiation, exhibiting a rounded cell shape, whereas control C2C12 cells underwent drastic morphological modifications toward multinucleated and elongated characteristic of myotubes (Fig. 13A bottom-left). Consistent with the cell morphology, in comparison to control C2C12 cells, ectopic Zfp516 expressing cells had a significant reduction in the expression of myogenic genes, including myogenic transcription factors, MyoG, MyoD, Myf6 and Myf5, as well as late markers MHC, TpnI and TpnT (Fig. 13A bottom right). These data show that ectopic expression of Zfp516 represses the myogenic program and drives transcription of a BAT gene program to promote brown adipocyte differentiation in C2C12 cells.

Next, we tested whether ablation of Zfp516 causes impairment of brown adipocyte differentiation *in vitro* by using mouse embryo fibroblasts (MEFs) isolated from Zfp516 $^{-/-}$embryos [28]. In contrast to wild-type that accumulated lipid droplets, knockout MEFs failed to differentiate as evidenced by lack of Oil red O (ORO) staining (Fig. 13B center-left). While the wild-type MEFs underwent a morphological change to the rounded polygonal shape characteristic of brown adipocytes, the knockout MEF retained fibroblast-like morphology (Fig. 13B center-left). UCP1 at both the protein and mRNA levels was greatly lower in the knockout MEFs (Fig. 13B center-left). Expression levels of other BAT-enriched genes, such as Cox8b, PGC1α, and Elovl3, were 50-80% lower in the knockout compared to wild-type MEFs (Fig. 13B top right). We next performed a rescue experiment using Zfp516 adenovirus in knockout MEFs. Compared to Zfp516 $^{-/-}$ MEFs, transduction with Zfp516 adenovirus completely rescued the phenotype in regard to morphological changes, lipid accumulation, and expression of BAT-enriched genes (Fig. 13B bottom). These data show that Zfp516 expression is necessary for differentiation of multipotent MEFs to brown adipocytes.

We next investigated whether knockdown of Zfp516 can inhibit BAT gene expression in brown preadipocyte cell line. HIB-1B cells were transduced with sh-Zfp516 or control lentivirus and the cells selected for stable integration were subjected to brown adipocyte differentiation. Zfp516 knockdown cells, which had approximately 50% lower Zfp516 mRNA (Fig. 13C center) and protein levels (Fig. 13C top-left) at confluence, showed drastically lower ORO staining after 5d of differentiation (Fig. 13C top-right). Similarly, Zfp516 knockdown resulted in a marked decrease in the expression of various BAT genes, including UCP1, PRDM16, PGC1α decreased by 70-90% and CideA, Elovl3

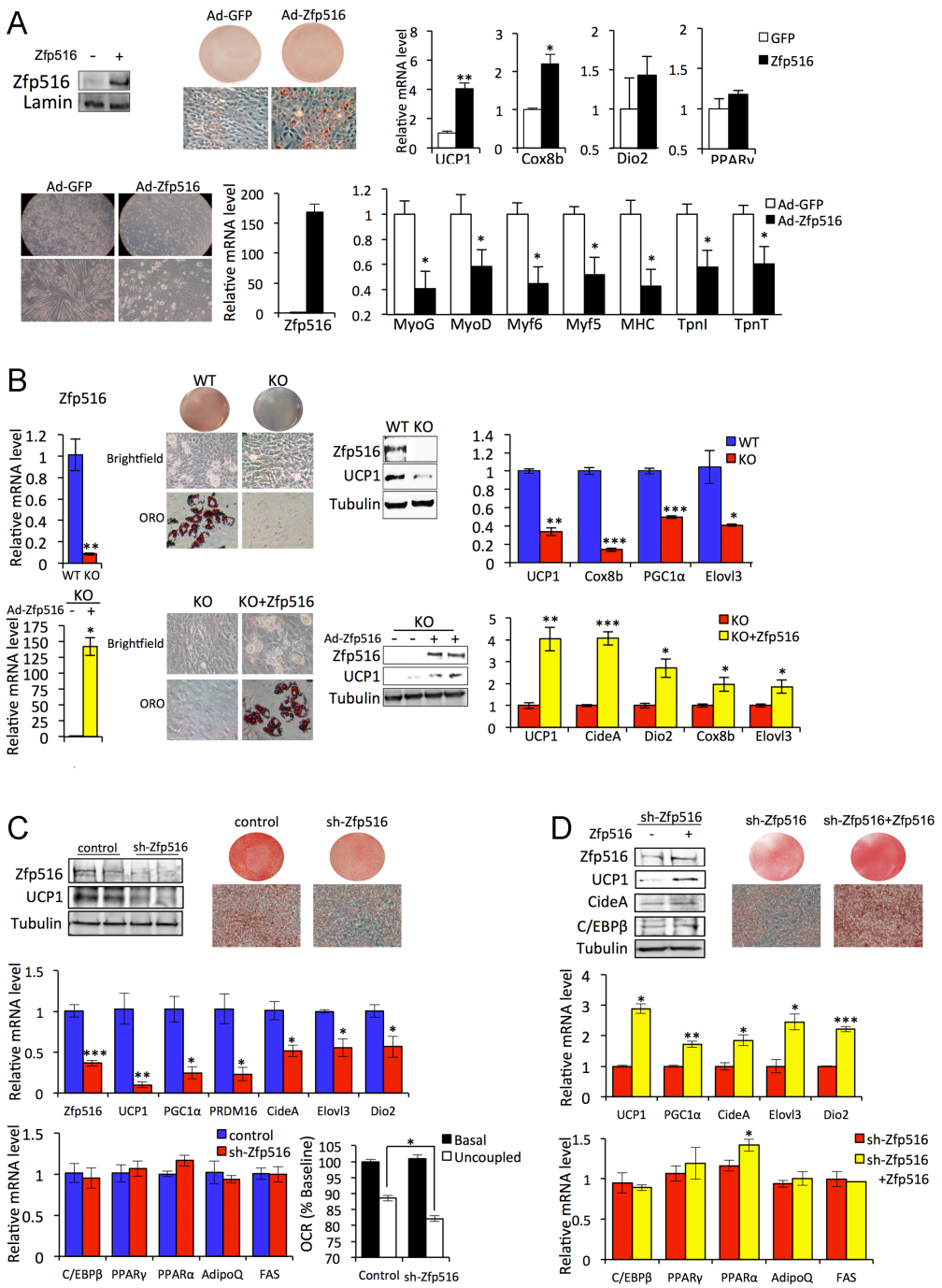


**Figure 13. Zfp516 promotes brown adipogenesis and suppresses myogenesis** A. Top, immunoblotting for indicated proteins (left), ORO staining (center) and RT-qPCR for BAT enriched genes and PPARγ (right) in C2C12 cells transduced with either GFP or Zfp516 adenovirus after 6 days of brown adipogenic differentiation. Bottom, Brightfield view at 20X (top left) and 40X (bottom left) magnification, RT-qPCR for Zfp516 mRNA (center), and RT-qPCR for muscle specific genes (right) in C2C12 cells transduced with GFP or Zfp516 adenovirus after 6d of myogenic differentiation. B. Top, RT-qPCR for Zfp516 mRNA (left), ORO staining and brightfield view pictures (center left), immunoblotting for indicated proteins (center right) and RT-qPCR for BAT enriched genes (right) in WT and KO MEFs after 5d of adipogenic

differentiation. Bottom, RT-qPCR for Zfp516 mRNA (left), ORO staining and brightfield view pictures (center left), immunoblotting for indicated proteins (center right) and RT-qPCR for BAT enriched genes (right) in KO MEFs infected with GFP or Zfp516 adenovirus after 5d of adipogenic differentiation. C. Top-left, immunoblotting for indicated proteins in HIB-1B cells infected with control or sh-Zfp516 lentivirus after 5d of adipogenic differentiation. Top-right, ORO staining at day 5 of differentiation. Middle, RT-qPCR for mRNA level of Zfp516 and BAT enriched genes these cells. Bottom-left, RT-qPCR for mRNA level of common adipogenic genes. Bottom-right, Relative OCR rates in cells before and after oligomycin treatment. OCR measurements before drug injection in the control cells were set as 100%. (N=9-10). D. Top-left, Immunoblotting for indicated proteins in sh-Zfp516 HIB-1B cells or sh-Zfp516 infected with Zfp516 adenovirus after 5 days of adipogenic differentiation. Top-right, ORO staining at day 5 of differentiation. Middle, RT-qPCR for BAT enriched genes. Bottom, RT-qPCR for common adipogenic genes. Error bars are +/- SEM. *$p<0.05$; **$p<0.01$; ***$p<0.001$.

and Dio2 by 40% (Fig. 13C middle) further indicating inhibition of brown adipocyte differentiation by Zfp516 knockdown. Gene expression levels of PPARγ, PPARα, AdipoQ and FAS, common markers for both WAT and BAT, were not affected (Fig. 13C bottom-left). We next measured the respiratory rates of the Zfp516 knockdown cells, to test if there was altered uncoupling in Zfp516 knockdown cells. While the basal respiratory rates were similar, the Zfp516 knockdown cells had significantly reduced uncoupling following oligomycin treatment compared to control cells (Fig. 13C bottom-right). These data show that Zfp516 is required for proper brown adipocyte differentiation *in vitro*, which can be reflected in mitochondrial uncoupling. Furthermore, in order to eliminate off-target effects of our shRNA knockdown, we performed a rescue experiment by infecting Zfp516 knockdown cells with adenoviral Zfp516. We observed a rescue of differentiation as evidenced by enhanced lipid accumulation (Fig. 13D top-right), increased expression of BAT enriched genes such as UCP1, CideA, PGC1α, Elovl3 and Dio2 at the mRNA level (Fig. 13D center) as well as at the protein level, while common adipocyte markers were unaffected (Fig. 13D bottom). Together these studies demonstrate that Zfp516 transcriptionally activates UCP1 and other BAT genes resulting in cell autonomous brown adipocyte differentiation.

## DISCUSSION

Due to its potential as a target of anti-obesity therapeutics, arising from evidenced presence of BAT like cells in humans, BAT development and activity have recently become an area of intense interest. While widely expressed transcription factors, such as PRDM16, PGC1α, C/EBPβ, and Ebf2, have been identified to promote the BAT program, specific brown fat enriched transcription factors may operate to activate BAT genes and BAT development [29]. By unbiased genome-wide transcription factor library screening, we identified the zinc-finger protein, Zfp516, as a novel brown fat enriched, cold-inducible DNA-binding transcriptional activator of UCP1 and other BAT genes, which promotes browning of iWAT and is required for BAT development. Importantly, we show that Zfp516 is induced by sympathetic signaling, which to our knowledge,

represents the first sympathetically regulated BAT-enriched transcription factor promoting a BAT program in iWAT and BAT.

The above-mentioned transcriptional activators act through the well-characterized enhancer element at -2.5kb upstream of UCP1 promoter. Indeed, the enhancer region found at -2.5kb along with the proximal -400bp of the UCP1 promoter has been found to be sufficient to drive reporter expression in a tissue specific and sympathetically regulated manner [16]. Here, we identified Zfp516 as a novel activator of the UCP1 promoter, through binding at the proximal promoter region. Interestingly, CREB has previously been identified to interact with the proximal promoter region at -140bp to activate the UCP1 promoter. However, even the proximal -120bp of the UCP1 promoter that does not contain a CRE has still shown to respond to sympathetic stimuli [30] clearly suggesting presence of a yet to be identified cold responsive transcription factors to function through binding to the proximal promoter region. Our finding that expression of Zfp516 is induced by cold and sympathetic stimulation and binds -70 to -45bp proximal region may represent such a transcription factor. In addition, Zfp516 can also bind PGC1α and Cox8b promoter regions for transcriptional activation. Zfp516 clearly acts as a transcriptional activator by binding to the promoter regions of BAT-enriched genes.

Recent research on the transcriptional factors critical for BAT development has centered on PRDM16. However, PRDM16 is broadly expressed and promotion of a BAT program by PRDM16 is independent of its DNA-binding activity [31,32]. Thus PRDM16 must act through other transcription factors that bind promoter regions of BAT-enriched genes. In this regard, PPARγ and C/EBPβ, which bind to the -2.5kb enhancer region, have been reported to function with PRDM16 to activate a BAT program [10,33] but these transcription factors also function in WAT development. Since the BAT program is induced upon cold exposure, DNA binding transcription factor(s) that are enriched in BAT and also cold inducible may act by interacting with PRDM16. We found that Zfp516, which binds to proximal promoter region of UCP1, directly interacts with PRDM16. In addition Zfp516 interacts with the PRDM16 ZF-2 domain that has been shown to interact with C/EBPβ [33]. The relationship between these transcription factors interacting with PRDM16 needs further studies. Regardless, unlike other PRDM16 interacting proteins, Zfp516 is cold inducible by the classical β-AR-PKA-CREB pathway. Zfp516 expression is induced by β-adrenergic stimulation in both BAT and iWAT depots by cold exposure as well as by β-agonist treatment. These results suggest that the transcriptional regulation of UCP1 in response to cold stimuli may require Zfp516 activity. Our finding that Zfp516 drives promoter activity of UCP1 and PGC1α, two genes both known to be essential for proper BAT response to cold [34,35], establishes the key role Zfp516 plays in transcriptional activation of BAT-genes during cold exposure.

We show here that overexpression of Zfp516 *in vivo* causes browning of iWAT, even at room temperature. While we cannot disregard a potential effect of Zfp516

in the central nervous system due to use of the aP2-promoter driving the transgene [36], the fact that Zfp516 is inducable by cold exposure for thermogenic genes activation indicates that Zfp516 may play a critical role in browning of iWAT. Sympathetic stimulation in mice causes Zfp516 levels to be an order of magnitude higher in iWAT but not in pWAT. However, we did not detect significant alterations in BAT phenotype in our transgenic mice. In this regard, although Zfp516 is also induced in BAT, the fold induction was significantly lower than that detected in iWAT. This may explain the inability of detecting changes in BAT in our transgenic mice. However, it is also possible that the endogenous Zfp516 level in BAT is sufficient for a BAT phenotype. Similar to our aP2-Zfp516 transgenic mice, overexpression of PRDM16 in adipose tissue caused browning of iWAT without alteration in BAT phenotype [37].

As Zfp516 directly interacts with PRDM16, this suggests that Zfp516 cooperatively works along with PRDM16 for browning of iWAT. Previously, PRDM16 presumptive BAT from null embryos was reported to have lower BAT enriched and higher muscle specific gene expression, with higher lipid stores. A recent report of a Myf5-cre PRDM16 conditional KO, however, indicated no defect in early BAT development but impaired BAT function in adults [38]. Although Zfp516 null embryonic presumptive BAT showed similar gene expression pattern to PRDM16 null, they also showed significantly decreased lipid staining, with altered genome-wide gene expression pattern as well as abnormal mitochondrial morphology. It is also possible that as a DNA binding protein, which often shows more severe phenotype of null mutation than coregulators, Zfp516 may interact with coregulator(s) other than PRDM16 during early BAT development.

Regardless, PRDM16 is expressed constitutively and, thus, the cold-inducible nature of Zfp516 could be a key driving BAT-gene program in browning of iWAT. Since iWAT is similar to human subcutaneous adipocytes, Zfp516, which induces browning of iWAT even at room temperature preventing diet induced obesity, may represent a compelling target for future anti-obesity therapeutics.

## EXPERIMENTAL PROCEDURES

### Antibodies, animals, and cell culture

All protocols for mice studies were approved from the University of California at Berkeley Animal Care and Use Committee. Mice were fed a chow diet ad libitum. Oxygen consumption ($VO_2$) was measured using the Comprehensive Laboratory Animal Monitoring System (CLAMS). Data were normalized to lean body mass as determined by MRI. Body temperatures were assessed using a RET-3 rectal probe for mice (Physitemp). CL316,243 (Sigma) was intraperitoneally injected into mice at 1mg/kg. GTT and ITT performed upon intraperitoneal injection of D-glucose 1mg/g or of insulin 0.75mU/g of

body weight as previously described [39]. Tail vein blood was collected for measurements. Derivation of mice is described in the supplementary methods.

Brown adipocyte differentiation was performed as described in [33]. To induce thermogenic genes, cells were treated for 6h with 10μM forskolin or 10μM isoproterenol. For myogenic differentiation, confluent cells were treated with DMEM containing 2% Horse serum and 25mM Hepes, pH 7.4. Primary MEFs were isolated as previously described [40]. MEF differentiation was performed as described in [28]. Cellular and tissue explant respiration was measured using a XF24 Analyzer (Seahorse Bioscience).

The following antibodies were used: ZNF516 (sc-85244 and sc-85244X (ChIP) , PGC1 (sc-13067), C/EBPβ (sc-7962), PPARγ (sc-7176), CideA (sc-8732), Lamin A (sc-20680), Tubulin (sc-5546), GAPDH (sc-32233) (all Santa Cruz), V5 (ab-9137) (Abcam), PRDM16 (pab19171) (Abnova), UCP1 (SAB2501082), FLAG M2 (F1804), anti-FLAG M2-HRP (A8592)(Sigma), and anti-V5-HRP (R96125) (Invitrogen).
Embryonic stem (ES) cell lines bearing a β-galactosidase-neomycin (β-geo) trap in the Zfp516 gene (Zfp516.β-geo) were from the German Gene Trap Consortium. The entire intron 1 of Znf516 gene and inserted β-geo region of the ES cell genomic DNA was sequenced to identify the exact insertion site. ES cells were microinjected into 3.5-day blastocysts derived from C57BL/6J females, and transferred to pseudopregnant C57BL/6J recipients. Chimeric mice were then bred with C57BL/6J mice for germline transmission. The mice were bred into C57BL/6J for at least 4 generations. The presence of the targeted allele in the black-colored offspring was confirmed by PCR.

293FT cells were grown in DMEM containing 10% fetal bovine serum, 1% penicillin/streptomycin, and 250μg/mL G418. HIB-1B brown preadipocytes, C2C12 myoblasts were grown in DMEM containing 10% FBS and 1% penicillin/streptomycin.

For adenoviral infection of MEFs, C2C12 or HIB-1B cells, subconfluent cells were incubated overnight with GFP or Zfp516 adenovirus. Viral medium is replaced with induction medium for brown adipogenic or myogenic conditions. Znf516 shRNA and or GFP control lentiviral particles (Santa Cruz) were transduced into HIB-1B cells. Cells were split 48 h post transduction and were selected with Puromycin (5ug/ml) for 5 days.

Briefly, HIB-1B cells seeded in XF24 plates were induced to differentiate as described above. On the day of experiments, the cells were washed once and maintained in XF-DMEM (Sigma-Aldrich) supplemented with 1 mM sodium pyruvate and 17.5 mM glucose. Oxygen consumption was blocked by 6 μM oligomycin. Maximal respiratory capacity was assayed by the addition of 8 μM FCCP. For tissue explants, tissues we excised and placed directly into KREB's-Heslinger buffer (121mM NaCl, 4.9mM KCl, 1.2mM $MgSO_4$, 0.33mM $CaCl_2$, 12mM Hepes, 25mM glucose, 10mM Sodium Pyruvate, 1% fatty acid free BSA, pH 7.4). 3-5μg pieces of tissue were put inXF-24 plates and secured using an islet capture screen. Tissues were incubated for 1 hr at 37°C without $CO_2$ prior to analysis on the XF24 Analyzer.

**Functional Screen**

cDNA clones from the Mammalian Genome Collection were cotransfected with the -5.5kb UCP1-eGFP-N1 into 293FT cells. Cells were assayed at 24 and 48hr post transfection for GFP signal. Positive clones were cotransfected with the -5.5kB UCP1-Luciferase construct into 293FT cells and assayed 24hr post transfection using the Dual-Luciferase Reporter assay (Promega). A more detailed protocol is included in the supplementary methods.

**Oil red O staining**

Wells were washed once with phosphate-buffered saline and subsequently fixed for 30min in 10% formalin. Cells were then stained with Oil Red O working solution for 1h. Cells were washed twice with distilled water prior to visualization.

**RT-PCR Analysis and Western blotting**

Total RNA was extracted using TRIzol reagent (Invitrogen). Reverse transcription was performed with 1μg of total RNA using SuperScript II (Invitrogen). RT-qPCR was performed in triplicate with an ABI PRISM 7500 sequence detection system (Applied Biosystems) to quantify the relative mRNA levels for various genes. Statistical analysis of the qPCR was obtained using the ΔΔCt method with U36B4 as the control. Primer sets used are listed in Table S1. Microarray hybridization and scanning were performed by the Functional Genomics Laboratory core facility using Affymetrix Mouse Genome 430A 2.0 Gene Chip arrays. Microarray data for both KO and TG mice are available at http://dx.doi.org/10.6084/m9.figshare.1009210 and http://dx.doi.org/10.6084/m9.figshare.1009211. For western blot analysis, total cell lysates were prepared using RIPA buffer and nuclear extracts were isolated using the NE-PER Nuclear and Cytoplasmic Extraction kit (Thermo). Proteins were separated by SDS-PAGE, transferred to nitrocellulose membrane and probed with the indicated antibodies.

**Luciferase Assays**

293FT cells were transfected with 300ng Zfp516 or empty vector and/or 300ng PRDM16 or empty vector in cotransfection assays together with 100 ng of indicated luciferase reporter construct and 0.5ng pRL-CMV in 24-well plates. Cells were lysed 24h post-transfection and assayed for luciferase activity as above.

**Transmission electron microscopy**

WT and KO BAT were fixed in 2% glutaraldehyde in 0.1M phosphate buffer, pH 7.3, at 4°C overnight, then postfixed in 1% $OsO_4$ and embedded in an Epon-Araldite mixture. Ultrathin sections (0.2μm) mounted on 150-mesh copper grids were stained with lead citrate and observed under a FEI Tecnai 12 transmission electron microscope.

**Plasmid Constructs**

The Zfp516 sequence was subcloned into FLAG/ pcDNA3.1. The 1-420 and 400-820 Zfp516 fragments were cloned into 3Tag-3a. The -5.5kb UCP1-GFP construct was generated by PCR amplifying the -5.5kb UCP1 promoter sequence from genomic DNA from C57BL/6 mouse liver and cloning into AseI/AgeI of eGFP-N1 (Clontech). The -5.5kb UCP1-Luc construct was generated by insertion of luciferase sequence into the Mfe-1/Age-1 sites of the 5.5kb UCP1-GFP construct, which removes GFP. The -1.5kb UCP1-luc, -500bp UCP1-luc, -150bp UCP1-luc, -70bp UCP1-luc, and -25bp UCP1-luc were generated by PCR amplifying the target region from genomic DNA and inserting into SacI/NheI of pGL2 basic vector (Promega). The -45bp and -70bp + enhancer constructs were generated by PCR amplifying the enhancers region and inserting into XmaI/KpnI of the pGL2 vectors described above. The -2.0kb PGC1a-luc and PRDM16 expression vectors were from Addgene.

**Functional Screen**

cDNA clones in pCMV-Sport6 vector from the Mammalian Genome Collection (Invitrogen) were screened for activation of the -5.5kb UCP1 promoter-eGFP-N1 construct. 100ng of -5.5kb UCP1-eGFP-N1, 1ng of lipofectamine2000 (Invitrogen), and 44.8µl Optimem (Gibco) were added to 40ng of test vector in 48-well plates. Complexes were added to7.5 X $10^4$ 293FT cells. Cells were assayed for GFP signal at 24 and 48h post-transfection. Each plate contained positive (pCMV-Sport6-CREB) and negative (pCMV-Sport6) controls. For secondary screening, 100ng of -5.5kb UCP1-Luciferase, 0.5ng pRL-CMV, and 1.2µl Lipofectamine2000 were diluted to 45µl in Optimem before addition of 50ng of each of the positive clone from the initial screen in 48-well plates in triplicates. 7.5 X $10^4$ 293FT cells were added to transfection mixtures and incubated for 24h. Cells were assayed for luciferase activity using Dual-Luciferase Reporter assay system (Promega).

**Cryosectioning and Immunostaining**

Fresh adipose tissue from indicated mice were embedded in OCT medium and snap-frozen. The tissue were sectioned on Leica CM3050S Cryostat in 10µm thick section and collected on Superfrost+ coated glass slides (Fisher). Briefly, slides were allowed to warm to room temperature for 5 minutes, fixed with 4% formalin phosphate buffered saline for 30 minutes at room temperature, blocked with 5% BSA in PBS containing 0.025% Triton X-100 (PBST), and incubated with the appropriate antibody diluted in 2.5% BSA in PBST overnight at 4°C. Slides were washed 3 times in PBST, and incubated with secondary antibody for 2 h at room temperature. Slides were then washed twice in PBST, and then stained with hematoxylin (bright field) for 30 s. Slides were washed and mounted in 15% glycerol in PBS with glass coverslips. Cell number and lipid

droplet area were quantified from fresh stained BAT, iWAT and pWAT slide pictures using ImageJ software (NIH opensource) and by counting a minimum of 100 cells in 4 random fields/picture/tissue and measuring 50 lipid droplets in 4 random fields/tissue.

**Electrophoretic Mobility Shift Assay**

Nuclear extracts of 293FT cells transfected with flag-Zfp516, flag-Zfp516 (AA1-420), or flag-Zfp516 (AA400-820) fragment were used in electrophoretic mobility shift assay (EMSA). Sense (5'-CCTGGGCCGGCTCAGCCACTTCCCCCAGTC-3') and antisense (5'-GACTGGGGGAAGTGGCTGAGCCGGCCCAGG-3') oligonucleotides were end-labeled by $\gamma$ $^{32}$P-ATP using T4 Polynucleotide kinase (NEB) or biotin (Thermo Scientific) and annealed. Samples were separated by 6% native PAGE before autoradiography or transferred to a nylon membrane and detected using streptavidin-HRP conjugate (Thermo Scientific).

**ChIP**

For ChIP analysis using 293FT cells, cells were transfected with 10 μg of either pcDNA3.1-FLAG-Zfp516 or Zfp516 truncations or pcDNA3.1 and 5 ug of either -5.5kb UCP1-Luciferase or -2kb PGC1α-Luciferase using calcium phosphate method. At 48 h post-transfection, cells were crosslinked for 10 min by adding 1% formaldehyde in DMEM at room temperature. Cross-linking was stopped by the addition of glycine to a final concentration of 0.125 M. After sonication, DNA sizes were 0.3–0.9kb. For HIB-1B cells, cells were cultured to confluence before crosslinking and sonication as above. For ChIP experiments in BAT, tissues were minced on ice and crosslinked using 1% formaldehyde in phosphate-buffered saline for 10 min. Crosslinking was stopped using glycine as before. Samples were dounced, washed twice, centrifuged and resuspended in RSB buffer, containing 10mM Tris pH 7.4, 10mM NaCl, 3mM $MgCl_2$, prior to sonication. Nuclei were released by douncing on ice and collected by centrifugation. Nuclei were then lysed in nuclei lysis buffer containing 50mM Tris, pH 8.0, 1% SDS 10mM EDTA supplemented with protease inhibitors, followed by sonication. Chromatin samples were diluted 1:10 with the dilution buffer, containing 16.7mM Tris, pH 8.1, 0.01% SDS 1.1 % Triton X-100 1.2mM EDTA and 1.67mM NaCl and proteinase inhibitors. Soluble chromatin was quantified by absorbance at 260 nm, and equivalent amounts of input DNA were immunoprecipitated using 5 μg of indicated antibodies or normal mouse IgG and protein A/G beads. After the beads were washed and cross-linking was reversed, DNA fragments were extracted with phenol-chloroform-isoamyl alcohol and chloroform-isoamyl alcohol. DNA was precipitated and resuspended in water. Samples were analyzed by endpoint and qPCR using the primer sets in Table S2.

**Co-IP**

293FT cells were transfected with 12.5 μg of Zfp516 expression vector and either PRDM16, C/EBPβ, PGC1α, or PPARγ using calcium phosphate method. 48 h post-transfection, nuclear extraction was carried out using the NE-PER Nuclear and Cytoplasmic Extraction kit (Thermo). Equal amounts of nuclear extracts were incubated with the specific antibodies and protein A/G agarose beads overnight at 4°C, washed and proteins separated by SDS-PAGE, transferred onto nitrocellulose membranes for immunoblotting.

For Co-IP experiments using tagged constructs, 293FT cells were transfected using Lipofectamine2000 to express FLAG-tagged Zfp516 and/or V5-tagged PRDM16. Cells were lysed in IP buffer containing 20 mM Tris, pH 7.4, 150 mM NaCl, 1mM EDTA, 10% glycerol, 1% NP-40 supplemented with proteases inhibitors. Total cell lysates were incubated 2 h at 4°C with either anti-FLAG M2 or anti-V5 -agarose beads (Sigma). Agarose beads were washed 3 times and bound proteins were eluted by boiling in Laemmli sample buffer and analysed by immunoblotting using the indicated antibodies.

For nuclear extracts in mice, BAT from mice was excised and miced finely in sterile PBS. Following centrifugation, PBS was removed and BAT was resuspended in CERI buffer from the NE-PER kit (Thermo). BAT was dounced 10 times with a loose mortar and filtered through a 100μm screen before continuing with manufacturer protocol.

***In vitro* Binding Assays**

GST-fused to various PRDM16 fragments (described in [22]) were expressed in BL21 by IPTG induction for 3 h at 37°C, purified on glutathione sepharose beads and eluted with elution buffer containing reduced glutathione. [$^{35}$S]-labeled Zfp516 protein was produced by using TNT coupled transcription/translation kit (Promega). 20 μg of GST fusion proteins were incubated overnight at 4°C with *in vitro* translated proteins and glutathione sepharose beads in a binding buffer containing 20mM Hepes, pH 7.7, 300mM KCl, 2.5mM $MgCl_2$, 0.05% NP40, 1mM DTT, and 10% glycerol. The sepharose beads were then washed 3 times with binding buffer. Bound proteins were eluted by boiling in Laemmli sample buffer, separated by SDS-PAGE and analysed by autoradiography.

**Statistical analysis.**

Data are expressed as means ± standard errors of the means (SEM). The statistical differences in mean values were assessed by Student's *t* test. All experiments were performed at least twice and representative data are shown.

**Table 1: List of Primers for RT-qPCR**

| Gene | Forward Primer | Reverse Primer |
|---|---|---|
| Adiponectin | GCA CTG GCA AGT TCT ACT GCA A | GTA GGT GAA GAG AAC GGC CTT GT |
| C/EBPβ | ACG ACT TCC TCT CCG ACC TCT | CGA GGC TCA CGT AAC CGT AGT |
| CideA | TGC TCT TCT GTA TCG CCC AGT | GCC GTG TTA AGG AAT CTG CTG |
| Cox8b | GAA CCA TGA AGC CAA CGA CT | GCG AAG TTC ACA GTG GTT CC |
| Dio2 | CAG TGT GGT GCA CGT CTC CAA TC | TGA ACC AAA GTT GAC CAC CAG |
| Elovl3 | TCC GCG TTC TCA TGT AGG TCT | GGA CCT GAT GCA ACC CTA TGA |
| FABP4 | ACA CCG AGA TTT CCT TCA AAC TG | CCA TCT AGG GTT ATG ATG CTC TTC A |
| FAS | TGC TCC CAG CTG CAG GC | GCC CGG TAG CTC CTG GGT GTA |
| FoxC2 | TGG AGG ACA GAG CCT TTT TCT T | GCG TAG CTC GAT AGG GCA G |
| Igfbp3 | CCA GGA AAC ATC AGT GAG TCC | GGA TGG AAC TTG GAA TCG GTC A |
| Mck | GCA AGC ACC CCA AGT TTG A | ACC TGT GCC GCG CTT CT |
| Myf5 | ATC CAG GTA TTC CCA CCT GCT | ACT GGT CCC CAA ACT CAT CCT |
| Myf6 | ATC AGC TAC ATT GAG CGT CTA CA | CCT GGA ATG ATC CGA AAC ACT TG |
| MyoD | CGC CAC TCC GGG ACA TAG | GAA GTC GTC TGC TGT CTC AAA GG |
| MyoG | AGC GCA GGT TCA AGA AAG TGA ATG | CTGTAGGCGCTCAATGTACTGGAT |
| Perilipin | TGT CAA TGC CTA TGA GAA GG | AGG GCG GGG ATC TTT TCC T |
| PGC1α | CCC TGC CAT TGT TAA GAC C | TGC TGC TGT TCC TGT TTT C |
| PPARα | GCG TAC GGC AAT GGC TTT AT | GAA CGG CTT CCT CAG GTT CTT |
| PPARγ | TCA GCT CTG TGG ACC TCT CC | ACC CTT GCA TCC TTC ACA AG |
| PRDM16 | CAG CAC GGT GAA GCC ATT C | GCG TGC ATC CGC TTG TG |
| TpnI | AGA GTG TGA TGC TCC AGA TAG C | AGC AAC GTC GAT CTT CGC A |
| TpnT | GGA ACG CCA GAA CAG ATT GG | TGG AGG ACA GAG CCT TTT TCT T |
| U36B4 | AGA TGC AGC AGA TCC GCA | GTT CTT GCC CAT CAG CAC C |
| UCP1 | ACT GCC ACA CCT CCA GTC ATT | CTT TGC CTC ACT CAG GAT TGG |
| VEGF | TAC TGC TGT ACC TCC ACC TCC ACC ATG | TCA CTT CAT GGG ACT TCT GCT CT |
| VEGFR1 | CGG AAG GAA GAC AGC TCA TC | CTT CAC GCG ACA GGT GTA GA |
| VEGFR2 | GGC GGT GGT GAC AGT ATC TT | TCT CCG GCA AGC TCA AT |
| Zfp516 | AGC GCT TGG ATA TCC TCA GTA | GAG GGG CCC TGC TGGCAC AGT |

**Table 2: List of Primers for ChIP**

| Target | Forward Primer | Reverse Primer |
|---|---|---|
| -70 UCP1 | TGT GGC CAG GGC TTT GGG AGT | AGA TTG CCC GGC ACT TCT GCG |
| -2.5kb UCP1 | AGC GTC ACA GAG GGT CAG T | GTG AGG CTG GAT CCC CAG A |
| -5kb UCP1 | ACA TTG CCA AGA CTG CGG CCA TC | ACC CCC AAA CAG CAG CAG CAA C |
| -150 PGC1α | AGC AAG CAA GCC ACA ACA CCC T | AGGGGTGGGGGCAGGTGAGT |
| -2.4 kb PGC1α | GCT CAC ACT GAA TTG TGG CAG GA | GGG CAG CGT GTC TGT GTT CA |
| -250 Cox8b | GGC TGA TCC ATC TCG CTG GCT GCT | CCC AAA CAC CGA GGC GCT GTG A |
| -2.8kb Cox8b | TGG CCC GAG CCC AGA AAG GCA GA | GAG GGA GGG CTC CGA TGG GGA GGT |

**Acknowledgements**
We thank Dr. S. Kajimura for GST-PRDM16 constructs and Dr. P. Tontonoz for the V5-PRDM16 construct. We thank D. Hunerdosse, J. Niliwat, W. Orenella, N. Chien, J. Zheng, X. Liang, E. Esquivel and J. Chong for technical assistance. The work was supported in part by DK095338 to H.S.S.

## REFERENCES


1. Cypess, A. M. *et al.* Identification and importance of brown adipose tissue in adult humans. *N. Engl. J. Med.* **360,** 1509–1517 (2009).

2. Farmer, S. R. Obesity: Be cool, lose weight. *Nature* **458,** 839–840 (2009).

3. Van Marken Lichtenbelt, W. D. *et al.* Cold-activated brown adipose tissue in healthy men. *N. Engl. J. Med.* **360,** 1500–1508 (2009).

4. Virtanen, K. A. *et al.* Functional brown adipose tissue in healthy adults. *N. Engl. J. Med.* **360,** 1518–1525 (2009).

5. Cederberg, A. *et al.* FOXC2 is a winged helix gene that counteracts obesity, hypertriglyceridemia, and diet-induced insulin resistance. *Cell* **106,** 563–573 (2001).

6. Leonardsson, G. *et al.* Nuclear receptor corepressor RIP140 regulates fat accumulation. *Proc. Natl. Acad. Sci. U. S. A.* **101,** 8437–8442 (2004).

7. Gensch, N., Borchardt, T., Schneider, A., Riethmacher, D. & Braun, T. Different autonomous myogenic cell populations revealed by ablation of Myf5-expressing cells during mouse embryogenesis. *Dev. Camb. Engl.* **135,** 1597–1604 (2008).

8. Lepper, C. & Fan, C.-M. Inducible lineage tracing of Pax7-descendant cells reveals embryonic origin of adult satellite cells. *Genes. N. Y. N 2000* **48,** 424–436 (2010).

9. Schulz, T. J. *et al.* Identification of inducible brown adipocyte progenitors residing in skeletal muscle and white fat. *Proc. Natl. Acad. Sci. U. S. A.* **108,** 143–148 (2011).

10. Seale, P. *et al.* PRDM16 controls a brown fat/skeletal muscle switch. *Nature* **454,** 961–967 (2008).

11. Rosenwald, M., Perdikari, A., Rülicke, T. & Wolfrum, C. Bi-directional interconversion of brite and white adipocytes. *Nat. Cell Biol.* (2013). doi:10.1038/ncb2740

12. Wu, J. *et al.* Beige adipocytes are a distinct type of thermogenic fat cell in mouse and human. *Cell* **150,** 366–376 (2012).

13. Waldén, T. B., Hansen, I. R., Timmons, J. A., Cannon, B. & Nedergaard, J. Recruited vs. nonrecruited molecular signatures of brown, 'brite,' and white adipose tissues. *Am. J. Physiol. Endocrinol. Metab.* **302,** E19–31 (2012).

14. Collins, S., Yehuda-Shnaidman, E. & Wang, H. Positive and negative control of Ucp1 gene transcription and the role of β-adrenergic signaling networks. *Int. J. Obes. 2005* **34 Suppl 1,** S28–33 (2010).

15. Kang, S. *et al.* Effects of Wnt signaling on brown adipocyte differentiation and metabolism mediated by PGC-1alpha. *Mol. Cell. Biol.* **25,** 1272–1282 (2005).

16. Ricquier, D. & Bouillaud, F. The mitochondrial uncoupling protein: structural and genetic studies. *Prog. Nucleic Acid Res. Mol. Biol.* **56,** 83–108 (1997).

17. Fulton, D. L. *et al.* TFCat: the curated catalog of mouse and human transcription factors. *Genome Biol.* **10,** R29 (2009).

18. Cassard-Doulcier, A. M. *et al.* Tissue-specific and beta-adrenergic regulation of the mitochondrial uncoupling protein gene: control by cis-acting elements in the 5'-flanking region. *Mol. Endocrinol. Baltim. Md* **7,** 497–506 (1993).

19. Laity, J. H., Lee, B. M. & Wright, P. E. Zinc finger proteins: new insights into structural and functional diversity. *Curr. Opin. Struct. Biol.* **11,** 39–46 (2001).

20. Cassard-Doulcier, A. M., Gelly, C., Bouillaud, F. & Ricquier, D. A 211-bp enhancer of the rat uncoupling protein-1 (UCP-1) gene controls specific and regulated expression in brown adipose tissue. *Biochem. J.* **333 ( Pt 2),** 243–246 (1998).

21. Kozak, U. C. *et al.* An upstream enhancer regulating brown-fat-specific expression of the mitochondrial uncoupling protein gene. *Mol. Cell. Biol.* **14,** 59–67 (1994).

22. Kajimura, S. *et al.* Regulation of the brown and white fat gene programs through a PRDM16/CtBP transcriptional complex. *Genes Dev.* **22,** 1397–1409 (2008).

23. Bachman, E. S. *et al.* βAR Signaling Required for Diet-Induced Thermogenesis and Obesity Resistance. *Science* **297,** 843–845 (2002).

24. Cannon, B. & Nedergaard, J. Brown adipose tissue: function and physiological significance. *Physiol. Rev.* **84,** 277–359 (2004).

25. Farmer, S. R. Molecular determinants of brown adipocyte formation and function. *Genes Dev.* **22,** 1269–1275 (2008).

26. Nedergaard, J. & Cannon, B. The changed metabolic world with human brown adipose tissue: therapeutic visions. *Cell Metab.* **11,** 268–272 (2010).

27. Nedergaard, J. & Cannon, B. The Browning of White Adipose Tissue: Some Burning Issues. *Cell Metab.* **20,** 396–407 (2014).

28. Tseng, Y.-H. *et al.* New role of bone morphogenetic protein 7 in brown adipogenesis and energy expenditure. *Nature* **454,** 1000–1004 (2008).

29. Rajakumari, S. *et al.* EBF2 determines and maintains brown adipocyte identity. *Cell Metab.* **17,** 562–574 (2013).

30. Rim, J. S. & Kozak, L. P. Regulatory motifs for CREB-binding protein and Nfe2l2 transcription factors in the upstream enhancer of the mitochondrial uncoupling protein 1 gene. *J. Biol. Chem.* **277,** 34589–34600 (2002).

31. Ohno, H., Shinoda, K., Ohyama, K., Sharp, L. Z. & Kajimura, S. EHMT1 controls brown adipose cell fate and thermogenesis through the PRDM16 complex. *Nature* **504,** 163–167 (2013).

32. Seale, P. *et al.* Transcriptional control of brown fat determination by PRDM16. *Cell Metab.* **6,** 38–54 (2007).

33. Kajimura, S. *et al.* Initiation of myoblast to brown fat switch by a PRDM16-C/EBP-beta transcriptional complex. *Nature* **460,** 1154–1158 (2009).

34. Leone, T. C. *et al.* PGC-1alpha deficiency causes multi-system energy metabolic derangements: muscle dysfunction, abnormal weight control and hepatic steatosis. *PLoS Biol.* **3,** e101 (2005).

35. Lin, J. *et al.* Defects in adaptive energy metabolism with CNS-linked hyperactivity in PGC-1alpha null mice. *Cell* **119,** 121–135 (2004).

36. Martens, K., Bottelbergs, A. & Baes, M. Ectopic recombination in the central and peripheral nervous system by aP2/FABP4-Cre mice: Implications for metabolism research. *FEBS Lett.* **584,** 1054–1058 (2010).

37. Seale, P. *et al.* Prdm16 determines the thermogenic program of subcutaneous white adipose tissue in mice. *J. Clin. Invest.* **121,** 96–105 (2011).

38. Harms, M. J. *et al.* Prdm16 Is Required for the Maintenance of Brown Adipocyte Identity and Function in Adult Mice. *Cell Metab.* **19,** 593–604 (2014).

39. Ahmadian, M. *et al.* Desnutrin/ATGL is regulated by AMPK and is required for a brown adipose phenotype. *Cell Metab.* **13,** 739–748 (2011).

40. Wang, Y. & Sul, H. S. Pref-1 regulates mesenchymal cell commitment and differentiation through Sox9. *Cell Metab.* **9,** 287–302 (2009).

# Chapter 3:

# Zc3h10 interacts in a transcription factor complex to activate the UCP1 promoter and non-shivering thermogenesis

**Zc3h10 interacts with Dot1l to drive UCP1 transcription and non-shivering thermogenesis**

## INTRODUCTION

The rapid increase in the prevalence of obesity and associated comorbidities such as type-2 diabetes, cancer, and cardiovascular disease in recent decades has necessitated the development of new anti-obesity treatments[1]. One promising avenue of has focused on stimulating brown adipose tissue (BAT), which recent research has shown to be prevalent and metabolically relevant in adult humans, to increase energy expenditure[2–5]. While white adipose tissue (WAT) primarily functions as the primary storages site of excess energy from the diet as triglycerides, BAT oxidizes both glucose and lipid to generate heat[6]. The thermogenic function of BAT is facilitated by a specialized inner mitochondrial $H^+$/ fatty acid symporter called Uncoupling Protein 1 (UCP1)[7]. In mice, expression of UCP1 is restricted to only BAT. However, upon prolonged cold exposure, $UCP1^+$ thermogenic adipocytes, termed "beige" or "brite" (Brown-in white) cells can arise in WAT depots, although whether this is from recruitment or transdifferentiation of white adipocytes is currently not well understood [8–10]. In adult humans, the expression pattern of thermogenic cells show similarity to either mouse beige or brown adipocytes depending on the depot surveyed[11–13]. Understanding the common thermogenic program for both populations will be important for generation of future anti-obesity therapeutics.

A multitude of transcriptional regulators have been implicated in the transcriptional regulation of UCP1, including transcription factors, Zfp516 and EBF2, transcriptional cofactors, PRDM16 and PGC1α, and the H3K9 methyltransferase, EHMT1[14–18]. However, an inclusive model for regulation of UCP1 transcription in both beige and brown adipocytes remains controversial. Early research on transcriptional regulation of the UCP1 promoter centered on the enhancer element located 2.5kb upstream of the UCP1 transcription start site[19,20]. However, recent evidence suggests that the proximal 5kb of the UCP1 promoter serves as a super enhancer (SE) and thus other factors may play an important role in regulating UCP1 transcription[21,22].

Previously performed high-throughput screening of transcriptional activators of the -5.5kb UCP1 promoter identified multiple previously unknown regulators of UCP1, including Zfp516, and a largely uncharacterized zinc-finger protein Zc3h10[14]. We here report that Zc3h10 is enriched in brown adipocytes where it binds and activates the UCP1 promoter at -4kb and is coactivated multiple transcriptional coregulators including the methyltransferase, Dot1l and the chromatin remodeling factor, Smarca5. We further show that Zfp516 in required for proper differentiation of brown adipocytes in culture. Furthermore, transgenic overexpression of Zc3h10 in adipose tissue results in prevention of diet induced obesity.

## RESULTS

### Zc3h10 binds and activates the distal UCP1 promoter

We originally identified Zc3h10 in our previously described screening efforts to identify transcriptional activators of the UCP1 promoter[14]. Zc3h10 was previously identified as putative tumor suppressor but the mechanism of action is unclear[23]. Motif analysis of Zc3h10 identified 3-N terminal CCCH-type zinc finger domains as well as a proline-rich domain near the C-terminus (Figure 14A). Members of the CCCH-type zinc finger family are largely uncharacterized, with only 26 of the 61 members found in the human genome (58 in mouse) having putative functions identified, the majority of which have been found to be involved in RNA metabolism (processing, splicing, stability). However, phylogenetic profiling and clustering of CCCH-type zinc fingers groups Zch3h10 with Toe1 and Dhx57, of which Toe1 has been reported to act as a transcriptional activator and the function of Dhx57 is currently unknown[24–26].

Tissue expression profiling of Zc3h10 by both RT-qPCR and immunoblotting show Zc3h10 to be enriched in BAT compared to other tissues assayed such as muscle and heart (Figure 14B left). Importantly, Zc3h10 is expressed 2 to 3 fold higher in BAT versus renal, inguinal, and perigonadal WAT depots (rWAT, iWAT, pWAT respectively) (Figure 14B middle). Further, Zc3h10 expression was over 4 fold higher in the adipocyte fraction than the stromal vascular fraction (SVF) in fractionated BAT (Figure 14B right). Similarly, we found that Zc3h10 levels increases over the course of brown adipocyte cell line differentiation, with a more rapid increase in both the mRNA and protein levels at from day 4 to 5 concomittant with an increase in UCP1 (Figure 14C). Other transcription factors involved in brown adipocyte function, PPARγ and PGC1α increase more gradually from day 2-5.

To begin to define how Zc3h10 activates the UCP1 promoter, we first sought to find the Zc3h10 binding site in the proximal UCP1 promoter. To do this, we performed chromatin immunoprecipitation (ChIP) on BAT from both wild type (WT) and transgenic mice expressing flag-Zc3h10 driven by the -5.4kb aP2 promoter, which will be characterized in detail below. ChIP using the flag antibody resulted in peak enrichment at the -4kb region of the UCP1 promoter, but not at the -2.5kb enhancer region or the proximal promoter (Figure 14D). To determine whether binding to this region results in activation of the UCP1 promoter, 1kb regions of the distal UCP1 promoter were cloned upsteam of the 70bp proximal promoter. Zc3h10 cotransfection with the -4.5kb to -3.5kb fragment resulted in ~2 fold activation while the -5.5kb to -4.5kb, -3.5 to -2.5, and the -2.5kb enhancer region fragments showed no significant increase in activity (Figure 14E). Together, these data show that Zc3h10 binds and activated the UCP1 promoter at -4kb to activate transcription.

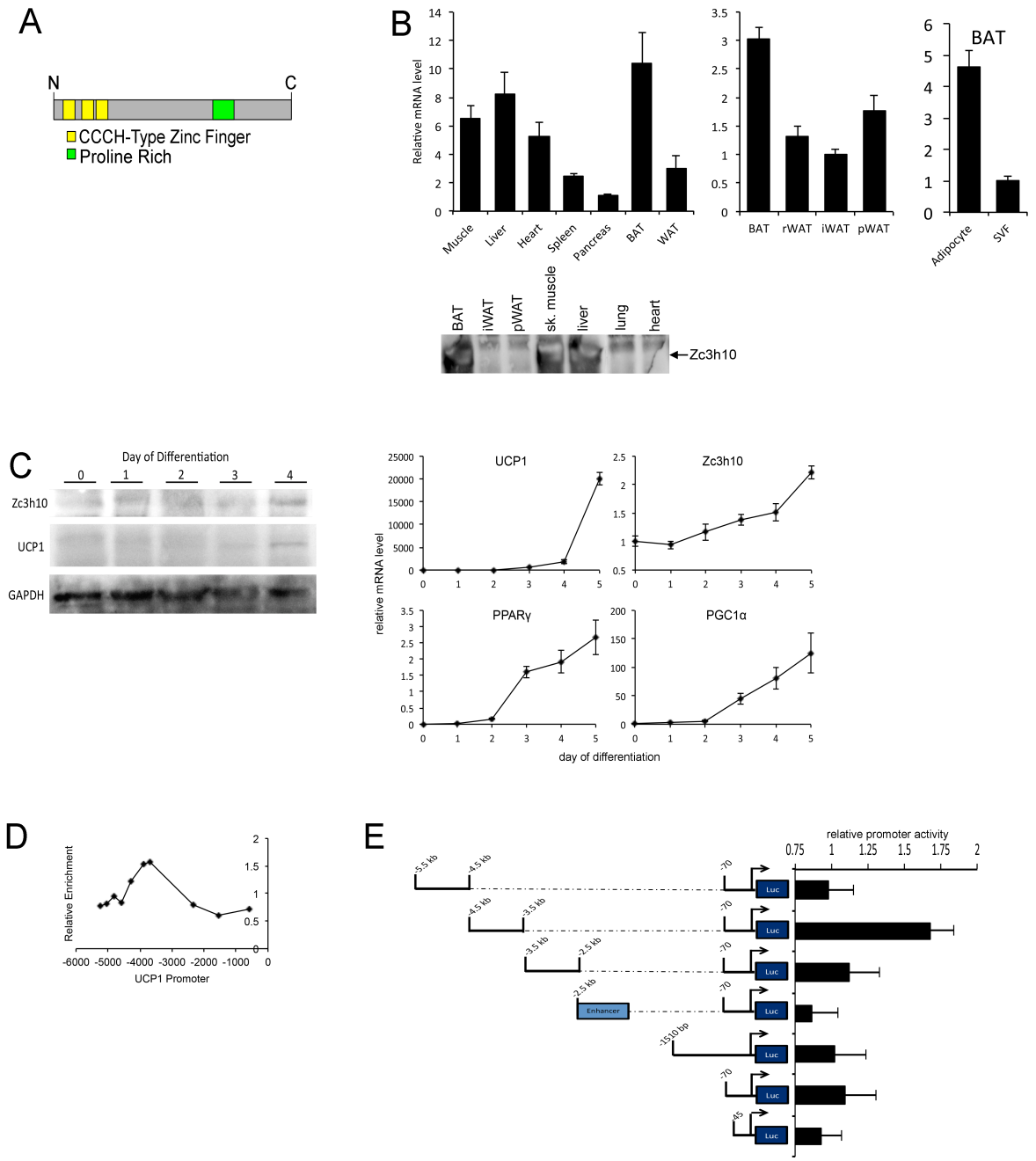


**Figure 14. Zc3h10 binds and activates the distal UCP1 promoter** A. Diagram of Zc3h10 structure. B. Left, RT-qPCR and immunoblotting for Zc3h10 in indicated tissues (left), adipose tissues (middle), and fractions of BAT (right). C. Immunoblotting (left) and RT-qPCR (right) for the indicated proteins over the course of BAT cell line differentiation. D. RT-qPCR quantification of ChIP DNA for the association of flag-Zc3h10 with the indicated region of the UCP1 promoter in BAT. E. Schematic representation of the fragments of the UCP1 promoter/ luciferase constructs and the relative promoter activity of indicated promoter constructs contrasfected with Zc3h10 in 293FT cells. Error bars are +/- SEM.

**Zc3h10 interacts with multiple transcription factors to activate the UCP1 promoter**

Transcription factors work as members of large complexes relaying binding of distal regulators and coregulators to Pol II at the transcription start site. To further elucidate how Zc3h10 regulates UCP1 transcription, we sought to identify Zc3h10 interacting partners in BAT. To do this, we performed tandem affinity purification (TAP) using Zc3h10 containing C-terminal streptavidin and calmodulin (TAP) epitope tags. Zc3h10 was purified from extracts of 293 cells and incubated with nuclear extracts from BAT. TAP-elutes were separated by SDS-PAGE and stained with commassie brilliant blue (CBB). Bands differentially found in Zc3h10-TAP eluates versus cTAP controls were identified by mass spectrometry (Figure 15A). We identified at least 7 polypeptides having molecular weights corresponding to the proteins identified by CBB staining. Interaction of these proteins, including SNW domain-containing 1 (Snw1), prohibitin (Phb), Dot1l, Smarca5, and Fused in Sarcoma (FUS) was then confirmed by coimmunoprecipitation of HA-tagged interacting proteins with flag-Zc3h10 (Figure 15B).

To determine whether these interacting partners affect Zc3h10 activation of the UCP1 promoter, we transfected each of these factors both individually and together with Zc3h10. Zc3h10 alone activated the UCP1 promoter over 4 fold as compared to empty vector controls while none of the identified interacting partner independently affected UCP1 promoter activity. Interestingly, when cotransfected with Zc3h10, Phb activated the UCP1 promoter over 10-fold, Smarca5 and Dot1l activated over 15-fold, and Snw1 activated the UCP1 promoter over 20-fold (Figure 15C). Each of these interacting partners synergistically activate the UCP1 promoter together with Zc3h10.

As none of these proteins have been associated with BAT function, we began to characterize the role of these proteins in thermogenesis. To begin, we measured the relative expression of these proteins in BAT and pWAT and found Dot1l to be enriched 2-fold in BAT compared to pWAT, Fus enriched 2-fold in pWAT, while Smarca5, Snw1, and Phb were similarly expressed in both tissues (Figure 15D). Further, we found expression of Zc3h10 interacting partners to increase over the course of BAT cell line differentiation (Figure 15E). We next looked at whether Zc3h10 interacting proteins are affected by acute cold exposure. We performed qPCR from BAT from cold exposed and room temperature control mice. Interestingly, only Smarca5 expression was higher in the cold exposed BAT while the other interacting factors were unchanged (Figure 15F). These data indicate that Zc3h10 interacting proteins may work together with Zc3h10 to activate the UCP1 promoter.

**Ablation of Zc3h10 inhibits brown adipocyte cell differentiation**

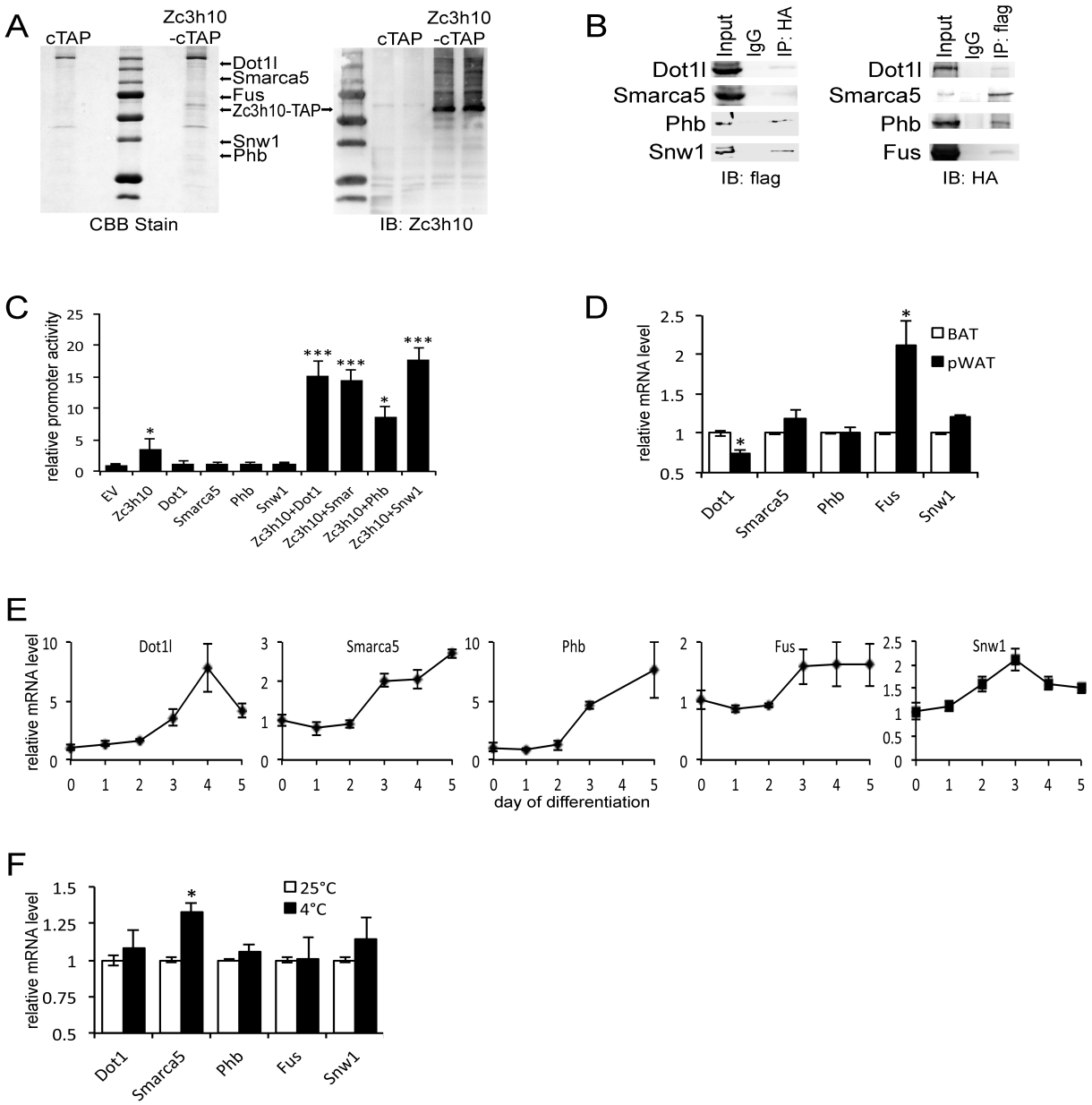


**Figure 15. Zc3h10 interacts with multiple transcription factors to activate the UCP1 promoter.** A. Left, purified Zc3h10 interacting proteins were separated by SDS-PAGE and stained with commassie brilliant blue (CBB). Unique bands identified by MS are indicated. Right, western blot for Zc3h10 showing Zc3h10-TAP expression. B. CoIP was performed on lysates of 293FT cells cotransfected with Zc3h10-flag and HA-tagged forms of the indicated proteins. Lysate were IPed for HA and blotted for flag (left) or IPed for flag and blotted for HA (right). C. Luciferase assay of 293FT cells transfected with the -5.5kB UCP1 promoter-luc and Zc3h10 and its interacting proteins alone or together with Zc3h10. Values are expressed relative to empty vector controls. D. RT-qPCR for the indicated genes in both BAT and pWAT. E. RT-qPCR of Zc3h10 interacting proteins over the course of BAT cell line differentiation. F. RT-qPCR of Zc3h10 interacting proteins in either RT or 6h cold exposed BAT. Error bars are +/- SEM. *p<0.05; ***p<0.001

As Zc3h10 can activate the UCP1 promoter *in vitro*, we next investigated whether ablation of Zc3h10 inhibits UCP1 expression in a brown preadipocyte cell line. BAT cells were transfected with Crispr/Cas9 constructs with either scrambled guide RNAs (gRNAs) or guides corresponding to the coding region of Zc3h10. Cells were selected for 5 days and clones were verified by sequencing and confirmed by western blotting (Figure 16 A; 16C left). Selected scambled and KO cell lines were then subject to brown adipocyte differentiation. Zc3h10 knock out cells show a drastic decrease in ORO staining indicative of decreased lipid accumulation (Figure 16B). Expression of BAT genes such as UCP1, PRDM16, Cox8b and Elovl3 were markedly lower in KO cells than in scrambled controls over the course of differentiation. At day 4 of differentiation, UCP1 expression is 80 fold lower in the KO cells while other BAT genes were repressed 3-4 fold (Figure 15C right). Protein levels of UCP1 and C/EBPβ were both virtually

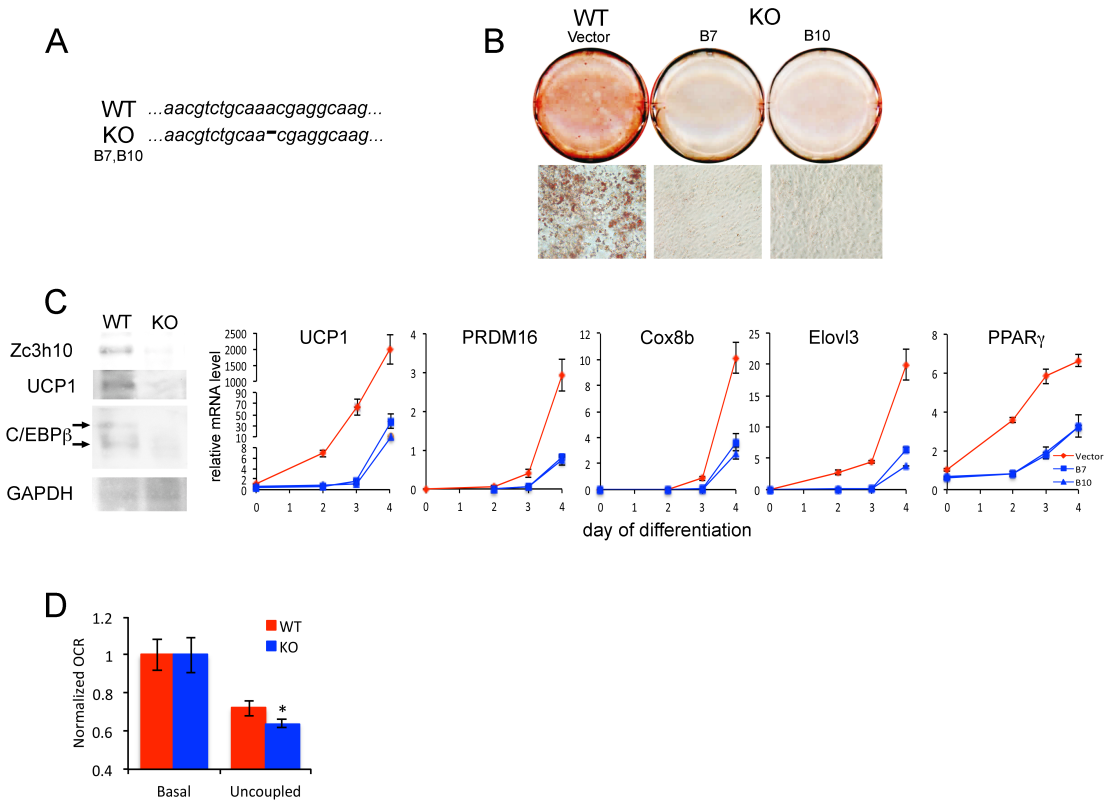


**Figure 16. Ablation of Zc3h10 inhibits brown adipocyte differentiation.** A. Genomic sequencing of Crispr mediated knockout cells identifying DNA sequence alteration. B. Oil Red O staining of vector (WT), B7 (KO), and B10 (KO) BAT cell line cells following 5 days of brown adipocyte differentiation. C. Left, western blotting for indicated proteins in lysates from WT and B7 KO cells as in B. Right, RT-qPCR for the indicated genes in WT and KO cells over the course of brown adipocyte differentiation. D. Relative OCR rates in cells before and after oligomycin treatment. OCR measurements before drug injection in the control cells were set as 100%. (N=9-10). Error bars are +/- SEM. *p<0.05.

undetectable at day 4 of differentiation (Figure 16C left). PPARγ expression, a marker of both white and brown adipocyte differentiation, was 2-3 fold lower in KO cells (Figure 15C right).

We next measured the respiratory rates of the Zc3h10 KO cells to test if there was altered uncoupling. When normalizing to basal oxygen consumption, we found that KO cells had reduced uncoupling following oligomycin treatment as compared to scramble control cells (Figure 16D). These data show that Zc3h10 ablation inhibits brown adipocyte differentiation, resulting in reduced uncoupling.

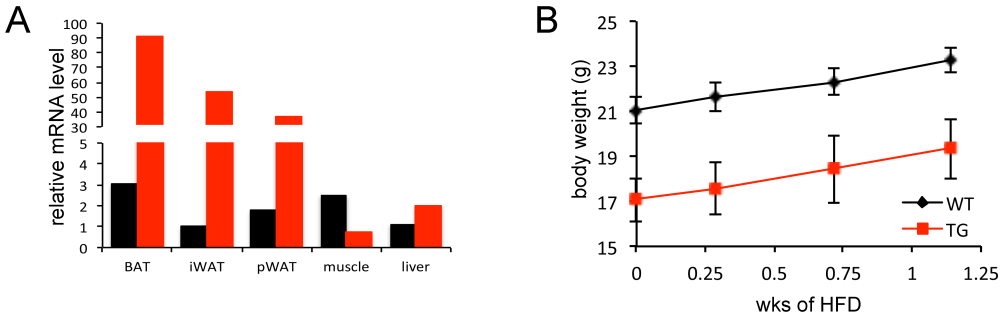


**Figure 17. Transgenic Zc3h10 expression prevents diet-induced obesity.** A. RT-qPCR for Zc3h10 in indicated tissues of wild-type (WT) and aP2-Zc3h10 transgenic mice (TG).(N=1) B. Body weight of WT and TG mice over the course of HFD feeding. (N=3-4). Error bars are +/- SEM.

**Transgenic Zc3h10 expression prevents diet-induced obesity**

To determine whether an increase in Zc3h10 expression results in an upregulation of UCP1 and BAT function *in vivo*, we generated transgenic mouse lines expressing Zfp516 driven by the -5.4kb aP2 promoter. As expected, Zc3h10 expression was 30-fold higher in transgenic BAT as compared to wild type BAT. Zc3h10 expression was 50-fold higher in iWAT and 20-fold higher in pWAT, although absolute levels are lower than in BAT. Zc3h10 expression in other tissues including muscle and liver were unchanged (Figure 17A). Interestingly, aP2-Zc3h10 transgenic mice have significantly smaller body weight compared to wild type littermates on chow diet at room temperature. When fed a palatable high fat diet, transgenic mice gain less weight (Figure 17B). These data indicate that transgenic Zc3h10 overexpression may increase energy expenditure to prevent diet induced obesity.

## DISCUSSION

Recent evidence of the prevalence and relevance of thermogenic adipocytes in human has resulted in increased interest in BAT. Better understanding of the hormonal and transcriptional circuits regulating BAT activity and development has the potential to identify new targets for novel obesity therapeutics. Using unbiased transcription factor library screening, we identified CCCH-type zinc finger protein, Zc3h10, as a novel

brown fat enriched transcriptional activator of UCP1. Furthermore, ablation of Zc3h10 blocks brown adipocyte differentiation and thus may be important for brown adipogenesis *in vivo*.

As mentioned above, the proximal 5kb of the UCP1 serves as a super enhancer, interacting with master transcription factors and the mediator complex, specifically including MED1[22,27]. Zc3h10 uniquely binds and activates the UCP1 promoter -4kb upstream of the TSS while the majority of factors act through the -2.5kb enhancer region. Thus, Zc3h10 may be the first member of an upstream UCP1 transcription factor complex. We further identified multiple binding partners for Zc3h10, all of which resulted in synergistic activation of the UCP1 promoter, perhaps representing a novel thermogenic regulatory complex. The list of interacting partners include 2 proteins with enzymatic activity: Dot1l and Smarca5. Dot1l catalyzes the methylation of histone H3 at lysine 79, a residue within the globular domain of the histone. Dot1l activity is almost universally associated with transcriptional activation and is rarely found in intergenic regions [28–30]. Smarca5, on the other hand, is the catalytic subunit of the ISWI chromatin remodeling complex and has been implicated in cell cycle progression, development, cell differentiation, and DNA damage response[31,32]. Neither of these factors, or the interacting transcription factors Fus, Snw1, and Phb have been found to be involved in thermogenesis and our results show that none of them are capable of independently activating the UCP1 promoter. However, together with Zc3h10, these proteins maybe essential for regulating of brown adipocyte development and/or regulation of thermogenesis.

Our preliminary experiments have shown that transgenic Zc3h10 expression in adipose tissues leads to a reduction in body weight. While this is likely a lean phenotype owing to increased energy expenditures in adipose tissue, we cannot disregard a potential developmental effect, as the aP2 promoter is active at various points during development. Similarly, aP2 is also active in the brain, further complicating the phenotype. Further study will be needed to characterize the mechanism responsible for the weight phenomenon is aP2-Zc3h10 mice. However, this is promising as it fits with our working hypothesis that Zc3h10 activates the UCP1 promoter leading to increased thermogenesis and increased energy expenditure. Thus, further work will be needed to determine whether Zc3h10 is a viable target for future obesity therapeutics.

## EXPERIMENTAL PROCEDURES

### Antibodies, animals, and cell culture

All protocols for mice studies were approved from the University of California at Berkeley Animal Care and Use Committee. Mice were fed a chow diet ad libitum. aP2-Zc3h10 mice were generated by cloning flag- Zc3h10 into -5.4kb aP2 promoter

pBluescript from addgene (plasmid #11424). Generation of mice was performed by Cyagen Biosciences.

Brown adipocyte differentiation was performed as described in [14]. Total RNA was extracted using TRIzol reagent (Invitrogen) on the days indicated. Wells used for ORO staining were washed once with phosphate-buffered saline and subsequently fixed for 30min in 10% formalin. Cells were then stained with Oil Red O working solution for 1h. Cells were washed twice with distilled water prior to visualization.

BAT cell line cells and 293FT cells were maintained in DMEM containing 10% FBS and 1% pen/strep prior to differentiation/ transfection. Crispr cells were generated by transfecting 10 cm plates at 70% confluence with BAT cell line cells with 10 μg of Crispr/Cas9 construct containing the gRNA sequence GCTGAGGAACGTCTGCAAACG using lipofectamine 3000 mediated transfection. Cells were washed once with warmed PBS 24 hr post transfection and fresh growth media was added. At 48hr post-transfection, cells were passaged 1:5 into growth media containing 0.8 μg/mL G418. Selection media was changed every 2 days. Cells were changed to regular growth media after 5 days of selection. After another 5-7 days, colonies were picked and grown in 96 well plates. gDNA of clones was isolated using the DNeasy kit (Qiagen) and amplified and sequenced using the following primers F- GGGGACCTCCTCCTTACCAT and R- CTTTCCGGAGGACCCCTTTC.

Briefly, BAT cell line cells seeded in XF24 plates were induced to differentiate as described above. On the day of experiments, the cells were washed twice and maintained in XF-DMEM (Sigma-Aldrich) supplemented with 1 mM sodium pyruvate and 17.5 mM glucose. Oxygen consumption was blocked by 1 μM oligomycin. Maximal respiratory capacity was assayed by the addition of 1 μM FCCP. Tissues were incubated for 1 hr at 37°C without $CO_2$ prior to analysis on the XF24 Analyzer.

293FT cells were transfected with 300ng Zfp516 or empty vector and/or 300ng or empty vector in cotransfection assays together with 100 ng of indicated luciferase reporter construct and 0.5ng pRL-CMV in 24-well plates. Cells were lysed 24h post-transfection and assayed for luciferase activity as above.

The following antibodies were used:, C/EBPβ (sc-7962), PPARγ (sc-7176), CideA (sc-8732), GAPDH (sc-32233) (all Santa Cruz), Zc3h10 (96-110), UCP1 (SAB2501082), FLAG M2 (F1804), anti-FLAG M2-HRP (A8592)(Sigma), and anti-HA (R96125) (Invitrogen).

**RT-PCR Analysis and Western blotting**

Reverse transcription was performed with 1μg of total RNA using SuperScript II (Invitrogen). RT-qPCR was performed in triplicate with an ABI PRISM 7500 sequence detection system (Applied Biosystems) to quantify the relative mRNA levels for various genes. Statistical analysis of the qPCR was obtained using the ΔΔCt method with U36B4 as the control. Zc3h10 primer sequence. Primer sets used are listed in table 3.

For western blot analysis, total cell lysates were prepared using RIPA buffer and nuclear extracts were isolated using the NE-PER Nuclear and Cytoplasmic Extraction kit (Thermo). Proteins were separated by SDS-PAGE, transferred to nitrocellulose membrane and probed with the indicated antibodies.

**Luciferase Assays**

293FT cells were transfected with 300ng Zc3h10 or empty vector and/or 300ng interacting partners or empty vector in cotransfection assays together with 100 ng of indicated luciferase reporter construct and 0.5ng pRL-CMV in 24-well plates. Cells were lysed 24h post-transfection and assayed for luciferase activity as above.

**Plasmid Constructs**

The Zc3h10 sequence was subcloned into 3Tag-3a. The -70, -70+ enhancer, -1.5kb, and -5.5kb UCP1-luciferase constructs were generated previously described[14]. The -5.5kb- -4.5kb+ -70 UCP1-luc, -4.5kb- -3.5kb+ -70 UCP1-luc, and -3.5kb- -2.5kb+ -70 UCP1-luc were generated by PCR amplifying the target region from genomic DNA and inserting into SacI/NheI of -70 UCP1-luc construct. (Promega). The HA-Smarca5, HA-Dot1l, HA-Fus, HA-Snw1, and HA-Phb expression vectors were purchased from Genecopeiea.

**ChIP**

For ChIP experiments in BAT, tissues were minced on ice and crosslinked using 1% formaldehyde in phosphate-buffered saline for 10 min. Crosslinking was stopped using glycine as before. Samples were dounced, washed twice, centrifuged and resuspended in RSB buffer, containing 10mM Tris pH 7.4, 10mM NaCl, 3mM $MgCl_2$, prior to sonication. Nuclei were released by douncing on ice and collected by centrifugation. Nuclei were then lysed in nuclei lysis buffer containing 50mM Tris, pH 8.0, 1% SDS 10mM EDTA supplemented with protease inhibitors, followed by sonication. Soluble chromatin was quantified by absorbance at 260 nm, and e1ug of input DNA was immunoprecipitated using 5 µg of indicated antibodies or normal mouse IgG and protein A/G beads. After the beads were washed and cross-linking was reversed, DNA fragments were extracted using a PCR-cleanup kit (Thermo Scientific). Samples were analyzed by qPCR using the primer sets in Table 3.

**Co-IP**

For Co-IP experiments using tagged constructs, 293FT cells were transfected using Lipofectamine2000 to express FLAG-tagged Zc3h10 and HA-tagged interacting proteins. Cells were lysed in IP buffer containing 20 mM Tris, pH 7.4, 150 mM NaCl, 1mM EDTA, 10% glycerol, 1% NP-40 supplemented with proteases inhibitors. Total cell lysates were incubated 2 h at 4°C with either anti-FLAG M2 or anti-HA agarose beads

(Sigma). Agarose beads were washed 3 times and bound proteins were eluted by boiling in Laemmli sample buffer and analysed by immunoblotting using the indicated antibodies.

**Statistical analysis.**

Data are expressed as means ± standard errors of the means (SEM). The statistical differences in mean values were assessed by Student's *t* test. All experiments were performed at least twice and representative data are shown.

**Acknowledgments**

We thank Dr. S. Kajimura for the BAT cell line. We thank D. Li, B. Bautista, J. Niliwat, E. Esquivel and J. Chong for technical assistance. The work was supported in part by DK095338 to H.S.S.

**Table 3: Primer Sets used for RT-qPCR**

| | Forward Primer | Reverse Primer |
|---|---|---|
| Zc3h10 | TTG TTG CTC CCA CAG GGG CAC | ACA GGA GCC ACA GGA GCC ACA |
| Dot1l | CTT GAC TTC TGG CAC CCG | TGC TGA CCA TGG AGT TGA GA |
| Smarca5 | GTC CAG AAC TGC GAT GGA GC | TTT CTT CCA CGG CCA TCA GG |
| Phb | GCG CAC GCG CAG TAT C | ACA GCT CTG TGT CCA GCA TC |
| Fus | TCA ATA AAT TTG GTG GTC CTC GG | GCC AGT TTC CCT GTC TGT GTA |
| Snw1 | TCC GTC ATG ACA GGC GAA AA | TCC ACT GTC CAT ACC CTT GGA |
| UCP1 ChIP 579/671 | CCA GGG CTC CTG CTA AGA AC | AGT GCA TCG TGT GGT CAC TT |
| UCP1 ChIP 1544/1697 | AAA CAT TGC CAA GAC TGC GG | TAT GTT GTG CAG GGC TTG GT |
| UCP1 ChIP 2345/2480 | CTG GGG ATA TCA GCC TCA CC | GAT GTC AAC TCA AGG CAG GGA |
| UCP1 ChIP 2901/2759 | TGG AAG CTG CAC ATT TCT GGA | GCT CCT CCC GTC GTA ACT TC |
| UCP1 ChIP 3227/3387 | ACT AGG AAG CAA ACC CAG AGC | GGC CAG AAA GAT GAT GCA GTG |
| UCP1 Chip 3674/3816 | CCC AAG CAG CTC TGT TCC TT | TCC AGT GGG TGA GGG TAG AT |
| UCP1 ChIP 4291/4446 | TTT CTG AGA GCT GGG TTG GC | TAG GCT GTA GGG CAC GTC AA |
| UCP1 ChIP 4815/4947 | AGC TAC TGG CAA GTC CCT GA | CAG TCT GGG ATG AAC CGG AG |
| UCP1 ChIP 5247/5394 | AGT TGT TGC ACA CCA CCC TT | CCA GTG GTA ACA ATA AAC ACC CG |
| UCP1 ChIP 5995/6124 | CAG TGA GCA CAC AAA CGA GTT C | CGA ACC ACT GTG GCC TCA AA |

## REFERENCES


1. Gesta, S., Tseng, Y.-H. & Kahn, C. R. Developmental origin of fat: tracking obesity to its source. *Cell* **131,** 242–256 (2007).

2. Cypess, A. M., Haft, C. R., Laughlin, M. R. & Hu, H. H. Brown fat in humans: consensus points and experimental guidelines. *Cell Metab.* **20,** 408–415 (2014).

3. Cypess, A. M. *et al.* Identification and importance of brown adipose tissue in adult humans. *N. Engl. J. Med.* **360,** 1509–1517 (2009).

4. Van Marken Lichtenbelt, W. D. *et al.* Cold-activated brown adipose tissue in healthy men. *N. Engl. J. Med.* **360,** 1500–1508 (2009).

5. Virtanen, K. A. *et al.* Functional brown adipose tissue in healthy adults. *N. Engl. J. Med.* **360,** 1518–1525 (2009).

6. Chondronikola, M. *et al.* Brown Adipose Tissue Improves Whole-Body Glucose Homeostasis and Insulin Sensitivity in Humans. *Diabetes* **63,** 4089–4099 (2014).

7. Fedorenko, A., Lishko, P. V. & Kirichok, Y. Mechanism of fatty-acid-dependent UCP1 uncoupling in brown fat mitochondria. *Cell* **151,** 400–413 (2012).

8. Long, J. Z. *et al.* A smooth muscle-like origin for beige adipocytes. *Cell Metab.* **19,** 810–820 (2014).

9. Wu, J., Cohen, P. & Spiegelman, B. M. Adaptive thermogenesis in adipocytes: is beige the new brown? *Genes Dev.* **27,** 234–250 (2013).

10. Wang, Q. A., Tao, C., Gupta, R. K. & Scherer, P. E. Tracking adipogenesis during white adipose tissue development, expansion and regeneration. *Nat. Med.* **19,** 1338–1344 (2013).

11. Jespersen, N. Z. *et al.* A classical brown adipose tissue mRNA signature partly overlaps with brite in the supraclavicular region of adult humans. *Cell Metab.* **17,** 798–805 (2013).

12. Cypess, A. M. *et al.* Anatomical localization, gene expression profiling and functional characterization of adult human neck brown fat. *Nat. Med.* **19,** 635–639 (2013).

13. Lidell, M. E. *et al.* Evidence for two types of brown adipose tissue in humans. *Nat. Med.* **19,** 631–634 (2013).

14. Dempersmier, J. *et al.* Cold-Inducible Zfp516 Activates UCP1 Transcription to Promote Browning of White Fat and Development of Brown Fat. *Mol. Cell* (2015). doi:10.1016/j.molcel.2014.12.005

15. Rajakumari, S. *et al.* EBF2 Determines and Maintains Brown Adipocyte Identity. *Cell Metab.* **17,** 562–574 (2013).

16. Ohno, H., Shinoda, K., Ohyama, K., Sharp, L. Z. & Kajimura, S. EHMT1 controls brown adipose cell fate and thermogenesis through the PRDM16 complex. *Nature* **504,** 163–167 (2013).

17. Seale, P. *et al.* PRDM16 controls a brown fat/skeletal muscle switch. *Nature* **454,** 961–967 (2008).

18. Kleiner, S. *et al.* Development of insulin resistance in mice lacking PGC-1α in adipose tissues. *Proc. Natl. Acad. Sci.* **109,** 9635–9640 (2012).

19. Cassard-Doulcier, A. M., Gelly, C., Bouillaud, F. & Ricquier, D. A 211-bp enhancer of the rat uncoupling protein-1 (UCP-1) gene controls specific and regulated expression in brown adipose tissue. *Biochem. J.* **333 ( Pt 2),** 243–246 (1998).

20. Shore, A., Karamitri, A., Kemp, P., Speakman, J. R. & Lomax, M. A. Role of Ucp1 enhancer methylation and chromatin remodelling in the control of Ucp1 expression in murine adipose tissue. *Diabetologia* **53,** 1164–1173 (2010).

21. Kong, X. *et al.* IRF4 is a key thermogenic transcriptional partner of PGC-1α. *Cell* **158,** 69–83 (2014).

22. Harms, M. J. *et al.* PRDM16 binds MED1 and controls chromatin architecture to determine a brown fat transcriptional program. *Genes Dev.* **29,** 298–307 (2015).

23. Guardiola-Serrano, F. *et al.* Gene trapping identifies a putative tumor suppressor and a new inducer of cell migration. *Biochem. Biophys. Res. Commun.* **376,** 748–752 (2008).

24. Sperandio, S., Tardito, S., Surzycki, A., Latterich, M. & de Belle, I. TOE1 interacts with p53 to modulate its transactivation potential. *FEBS Lett.* **583,** 2165–2170 (2009).

25. Liang, J., Song, W., Tromp, G., Kolattukudy, P. E. & Fu, M. Genome-Wide Survey and Expression Profiling of CCCH-Zinc Finger Family Reveals a Functional Module in Macrophage Activation. *PLoS ONE* **3,** e2880 (2008).

26. Hwang, E. S., Choi, A. & Ho, I.-C. Transcriptional regulation of GATA-3 by an intronic regulatory region and fetal liver zinc finger protein 1. *J. Immunol. Baltim. Md 1950* **169,** 248–253 (2002).

27. Whyte, W. A. *et al.* Master transcription factors and mediator establish super-enhancers at key cell identity genes. *Cell* **153,** 307–319 (2013).

28. Steger, D. J. *et al.* DOT1L/KMT4 Recruitment and H3K79 Methylation Are Ubiquitously Coupled with Gene Transcription in Mammalian Cells. *Mol. Cell. Biol.* **28,** 2825–2839 (2008).

29. Bernt, K. M. *et al.* MLL-Rearranged Leukemia Is Dependent on Aberrant H3K79 Methylation by DOT1L. *Cancer Cell* **20,** 66–78 (2011).

30. Barski, A. *et al.* High-Resolution Profiling of Histone Methylations in the Human Genome. *Cell* **129,** 823–837 (2007).

31. Armas, P., Margarit, E., Mouguelar, V. S., Allende, M. L. & Calcaterra, N. B. Beyond the binding site: in vivo identification of tbx2, smarca5 and wnt5b as molecular targets of CNBP during embryonic development. *PloS One* **8,** e63234 (2013).

32. Smeenk, G. *et al.* Poly(ADP-ribosyl)ation links the chromatin remodeler SMARCA5/SNF2H to RNF168-dependent DNA damage signaling. *J. Cell Sci.* **126,** 889–903 (2013).

Chapter 4:

# Conclusion

The meteoric rise in obesity and related diseases including cardiovascular disease, metabolic syndrome, and diabetes affects not only quality of life but also creates a large burden on the health care system[1]. Most recent CDC estimates show the costs of obesity in the U.S. to be in excess of $147 billion per year (http://www.cdc.gov/obesity/data/adult.html). This has created a burning need to identify and develop novel obesity therapeutics. One promising area of research has centered on the activity of brown adipose tissue (BAT). Through the activity of a specialized mitochondrial proton/ fatty acid symporter called uncoupling protein 1 or UCP1, BAT is able to dissipate the proton-motive force created by the electron transport chain to generate heat instead of ATP, a process known as uncoupled respiration (Figure 18A)[2–4]. Recent reports have shown the beneficial effects of increases BAT activity including improved glucose and lipid clearance, improved insulin sensitivity, as well as correlating loss in body fat, in both mice and men[5–7]. However, fundamental questions regarding regulation of BAT in humans persist, and while mouse models have help identify regulators of BAT development and activity, an inclusive model for regulation of thermogenesis remains unclear.

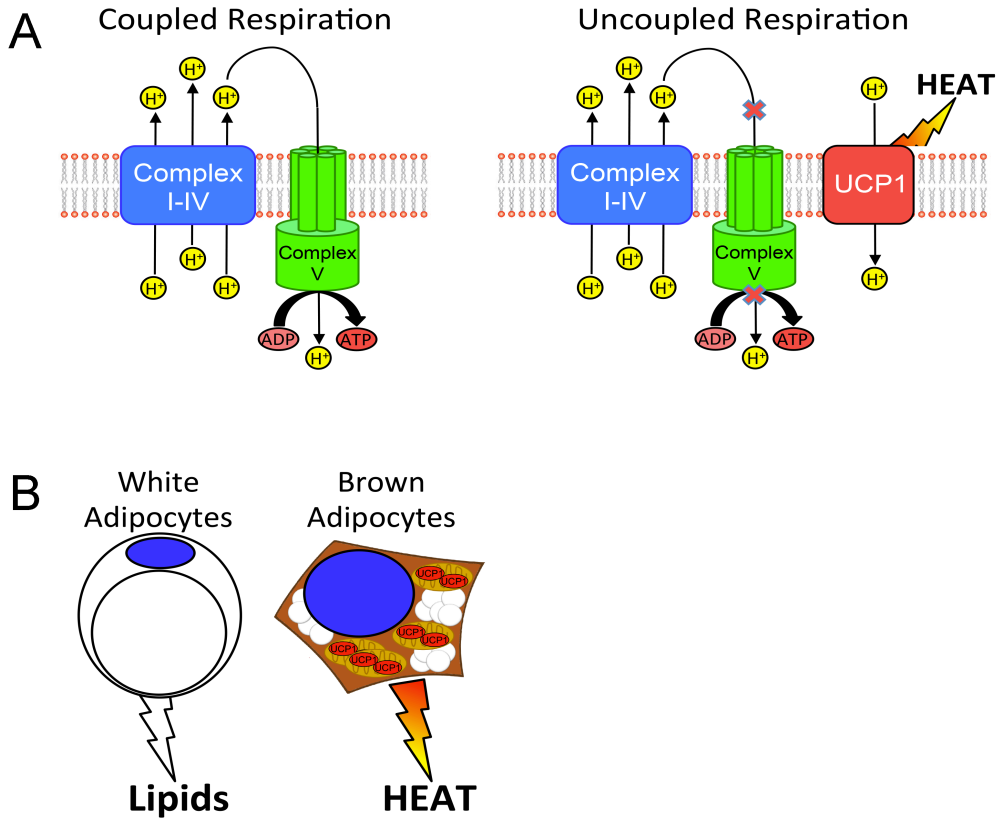


**Figure 18. Uncoupled Respiration and Brown Adipose Tissue.** A. Schematic representation of both coupled and uncoupled respiration including UCP1 activity. B. Schematic representation of the functional differences of brown and white adipocytes.

In contrast to BAT, white adipose tissue (WAT) stores excess dietary calories as triglyceride and releases lipolyzed fatty acids during periods of fasting (Figure 18B)[8]. More recent studies have shown that WAT also functions as an essential endocrine organ, releasing adipokines to maintain energy homeostasis[9,10]. WAT can also play a critical role in thermogenesis. In response to chronic cold exposure, UCP1$^+$ brown adipocyte-like cells arise in white adipose depots complete with increased mitochondrial content, multilocular lipid droplets, and increased vascularization and sympathetic innervation[11,12]. These so called "beige" or "brite" (brown in white) adipocytes provide excess thermogenic capacity for cold adaptation in rodents although the contribution to whole body thermogenic capacity is not well understood[13,14]. Contrary to classical BAT, following removal of the cold stress, these brown adipocyte-like cells revert back to a more classical UCP1$^-$ white adipocyte. Further cold stresses result in interconversion of these cells back to brown adipocyte-like cells[15]. Outside of a few rare cases in outdoor workers in cold climates, adult humans have long been thought to lack brown adipose tissue[16]. However, in 2009, multiple groups identified metabolically active and relevant UCP1$^+$ brown adipocytes using FDG-PET scanning[5,17–19]. Later work has revealed that human BAT more closely resembles the inducible brown adipocyte-like cells in the mouse although different depots within the same anatomical region can more closely resemble classical WAT or BAT in the mouse [6,20,21]. While the process of "browning" requires additional levels of regulation, common regulatory mechanisms of thermogenesis likely exist.

As the UCP1 protein is central to nonshivering thermogenesis in both BAT and brown adipocyte-like cells, we performed unbiased screening a library of transcription factors against the proximal 5.5kb of the UCP1 promoter to identify regulators of nonshivering thermogenesis. Our initial screening efforts identified 18 novel transcriptional regulators of UCP1, of which, 6 are enriched in BAT versus WAT. We have made major progress characterizing to role of 2 of the identified proteins in nonshivering thermogenesis, Zfp516 and Zc3h10. Zfp516 is a C2H2 type zinc finger protein. We found that Zfp516 was induced by cold, where it binds and activates the proximal UCP1 promoter as well as the PGC1α and Cox8b promoters. Further, Zfp516 directly interacts with PRDM16, whose activity has been shown to be required for the recruitment of brown adipocyte-like cells and plays a role is the regulation of BAT thermogenesis as well, although the extent to which it is required is unclear[22–24]. Zfp516 recruits PRDM16 to target BAT promoters to drive expression. Ablation of Zfp516 causes a drastic reduction in BAT with no UCP1 expression, altered morphology, and drastically reduced lipid accumulation. Conversely, transgenic overexpression of Zfp516 under control of the adipose specific aP2 promoter resulted in a drastic browning of the inguinal WAT resulting in an increased body temperature, whole body energy expenditure, and prevention of diet-induced obesity.

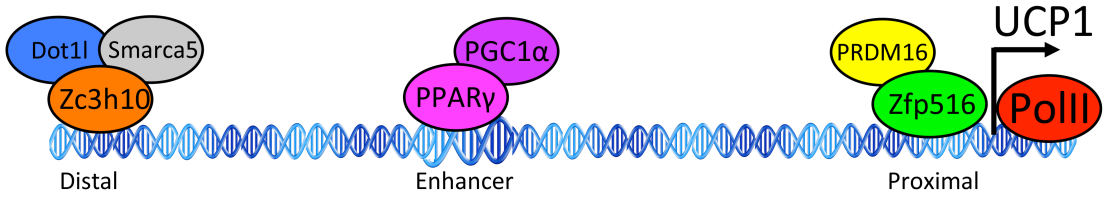


**Figure 19. Transcriptional Regulators of the UCP1 Promoter.** Schematic representation of UCP1 promoter depicting transcriptional regulators and coregulators discussed in the text.

We have also made significant progress characterizing the second transcription factor from our screen, the CCCH-type zinc finger protein, Zc3h10. Unlike Zfp516, which binds at the proximal UCP1 promoter, Zc3h10 binds 4 kb upstream of the UCP1 transcription start site, where it binds multiple transcriptional regulators including the H3K79 methyltransferase, Dot1L, and the chromatin remodeler, Smarca5, as well as other transcription factors. These interactions result in synergistic activation of the UCP1 promoter. We have further shown that transgenic Zc3h10 expression under control of the aforementioned aP2 promoter results in significant reduction in body weight. The mechanism for this lower body weight is currently unclear.

Through our work here, we have identified multiple novel transcriptional regulators of UCP1 and nonshivering thermogenesis. These data present many potential targets and pathways with therapeutic potential as well as new markers of the brown adipocyte thermogenic program. More work is necessary to determine the role of these genes in human brown adipocytes.

REFERENCES


1. Gesta, S., Tseng, Y.-H. & Kahn, C. R. Developmental origin of fat: tracking obesity to its source. *Cell* **131,** 242–256 (2007).

2. Fedorenko, A., Lishko, P. V. & Kirichok, Y. Mechanism of fatty-acid-dependent UCP1 uncoupling in brown fat mitochondria. *Cell* **151,** 400–413 (2012).

3. Cannon, B. & Nedergaard, J. Brown adipose tissue: function and physiological significance. *Physiol. Rev.* **84,** 277–359 (2004).

4. Nedergaard, J. *et al.* UCP1: the only protein able to mediate adaptive non-shivering thermogenesis and metabolic inefficiency. *Biochim. Biophys. Acta BBA - Bioenerg.* **1504,** 82–106 (2001).

5. Cypess, A. M. *et al.* Identification and importance of brown adipose tissue in adult humans. *N. Engl. J. Med.* **360,** 1509–1517 (2009).

6. Cypess, A. M. *et al.* Anatomical localization, gene expression profiling and functional characterization of adult human neck brown fat. *Nat. Med.* **19,** 635–639 (2013).

7. Chondronikola, M. *et al.* Brown Adipose Tissue Improves Whole-Body Glucose Homeostasis and Insulin Sensitivity in Humans. *Diabetes* **63,** 4089–4099 (2014).

8. Cinti, S. The adipose organ. *Prostaglandins Leukot. Essent. Fatty Acids* **73,** 9–15 (2005).

9. Ouchi, N., Parker, J. L., Lugus, J. J. & Walsh, K. Adipokines in inflammation and metabolic disease. *Nat. Rev. Immunol.* **11,** 85–97 (2011).

10. Berg, A. H. & Scherer, P. E. Adipose Tissue, Inflammation, and Cardiovascular Disease. *Circ. Res.* **96,** 939–949 (2005).

11. Bagchi, M. *et al.* Vascular endothelial growth factor is important for brown adipose tissue development and maintenance. *FASEB J. Off. Publ. Fed. Am. Soc. Exp. Biol.* (2013). doi:10.1096/fj.12-221812

12. Bartness, T. J., Vaughan, C. H. & Song, C. K. Sympathetic and sensory innervation of brown adipose tissue. *Int. J. Obes. 2005* **34 Suppl 1,** S36–42 (2010).

13. Schulz, T. J. *et al.* Brown-fat paucity due to impaired BMP signalling induces compensatory browning of white fat. *Nature* **495,** 379–383 (2013).

14. Cinti, S. The adipose organ: morphological perspectives of adipose tissues. *Proc. Nutr. Soc.* **60,** 319–328 (2001).

15. Rosenwald, M., Perdikari, A., Rülicke, T. & Wolfrum, C. Bi-directional interconversion of brite and white adipocytes. *Nat. Cell Biol.* (2013). doi:10.1038/ncb2740

16. Huttunen, P., Hirvonen, J. & Kinnula, V. The occurrence of brown adipose tissue in outdoor workers. *Eur. J. Appl. Physiol.* **46,** 339–345 (1981).

17. Van Marken Lichtenbelt, W. D. *et al.* Cold-activated brown adipose tissue in healthy men. *N. Engl. J. Med.* **360,** 1500–1508 (2009).

18. Virtanen, K. A. *et al.* Functional brown adipose tissue in healthy adults. *N. Engl. J. Med.* **360,** 1518–1525 (2009).

19. Farmer, S. R. Obesity: Be cool, lose weight. *Nature* **458,** 839–840 (2009).

20. Wu, J. *et al.* Beige adipocytes are a distinct type of thermogenic fat cell in mouse and human. *Cell* **150,** 366–376 (2012).

21. Jespersen, N. Z. *et al.* A classical brown adipose tissue mRNA signature partly overlaps with brite in the supraclavicular region of adult humans. *Cell Metab.* **17,** 798–805 (2013).

22. Cohen, P. *et al.* Ablation of PRDM16 and beige adipose causes metabolic dysfunction and a subcutaneous to visceral fat switch. *Cell* **156,** 304–316 (2014).

23. Harms, M. J. *et al.* Prdm16 Is Required for the Maintenance of Brown Adipocyte Identity and Function in Adult Mice. *Cell Metab.* **19,** 593–604 (2014).

24. Seale, P. *et al.* Prdm16 determines the thermogenic program of subcutaneous white adipose tissue in mice. *J. Clin. Invest.* **121,** 96–105 (2011).